

## Abstract

Title of Document: STRESS RESPONSE OF BOVINE ARTERY AND RAT  
BRAIN TISSUE DUE TO COMBINED TRANSLATIONAL  
SHEAR AND FIXED UNCONFINED COMPRESSION  
DEFORMATION

Lauren Leahy, M.S. Mechanical Engineering, 2015

Directed By: Dr. Henry W. Haslach, Jr., Mechanical Engineering

During trauma resulting from impacts and blast waves, sinusoidal waves permeate the brain and cranial arterial tissue, both non-homogeneous biological tissues with high fluid contents. The experimental shear stress response to sinusoidal translational shear deformation at 1 Hz and 25% strain amplitude and either 0% or 33% compression is compared for rat brain tissue and bovine aortic tissue. Both tissues exhibit Mullins effect in shear. Harmonic wavelet decomposition, a novel application to the mechanical response of these tissues, shows significant 1 Hz and 3 Hz components. The 3 Hz component magnitude in brain tissue, which is much larger than in aortic tissue, may correlate to interstitial fluid induced drag forces that decrease on subsequent cycles perhaps because of damage resulting in easier fluid movement. The fluid may cause the quasiperiodic, viscoelastic behavior of brain tissue. The mechanical response differences under impact may cause shear damage between arterial and brain connections.

STRESS RESPONSE OF BOVINE ARTERY AND RAT BRAIN TISSUE  
DUE TO COMBINED TRANSLATIONAL SHEAR AND FIXED  
UNCONFINED COMPRESSION

By

Lauren Leahy

Thesis submitted to the Faculty of the Graduate School of the  
University of Maryland, College Park in partial fulfillment  
of the requirements for the degree of  
Masters of Science  
2015

Advisory Committee:  
Dr. Henry W. Haslach, Jr., Chair  
Dr. Balakumar Balachandran  
Dr. Amr Baz

© Copyright by  
Lauren Leahy  
2015

# Contents

<b>1</b>	<b>Introduction</b>	<b>1</b>
<b>2</b>	<b>Background</b>	<b>3</b>
2.1	Phase shift . . . . .	3
2.2	Tissue Structure . . . . .	7
2.2.1	Artery . . . . .	8
2.2.2	Rat Brain . . . . .	13
2.3	Mullins Effect . . . . .	17
<b>3</b>	<b>Methods</b>	<b>19</b>
3.1	Apparatus . . . . .	19
3.2	Specimen Preparation . . . . .	20
3.2.1	Aorta . . . . .	20
3.2.2	Brain . . . . .	21
3.3	Protocol . . . . .	27
3.3.1	Combined Sinusoidal Translational Shear and Fixed Initial Unconfined Compression . . . . .	28
3.4	Methods of Analysis . . . . .	28
3.4.1	Mullins Effect . . . . .	29
3.4.2	Signal Processing Analysis . . . . .	29
3.4.3	Statistical Analysis . . . . .	33
<b>4</b>	<b>Results</b>	<b>35</b>
4.1	Qualitative Analysis . . . . .	35
4.1.1	First Peak Amplitude of Sinusoidal Shear Response . . . . .	38
4.1.2	Mullins Effect in Shear Stress Response to Translational Shear Deformation . . . . .	38
4.1.3	Symmetry of one Load-Unload Cycle . . . . .	43
4.1.4	Symmetry about the Horizontal Axis . . . . .	44
4.1.5	Time Shift . . . . .	44
4.1.6	Limit Cycle . . . . .	48
4.2	Frequency Decomposition of the Stress Response . . . . .	51
4.2.1	Frequency Filter . . . . .	51
4.2.2	Fourier Series Analysis . . . . .	53
4.2.3	Harmonic Wavelet Analysis . . . . .	59
4.2.4	2 Hz Analysis . . . . .	66
4.2.5	Results Summary . . . . .	68
<b>5</b>	<b>Discussion</b>	<b>69</b>
5.1	Solid-Fluid Interaction in the Mechanical Response . . . . .	73
5.2	Transient Response . . . . .	74
5.3	Frequency Analysis . . . . .	75

	iii	
5.3.1	Fluid Influence on Brain Tissue Response during a Load-Unload Deformation Cycle . . . . .	76
5.3.2	Aortic Tissue Stress Response . . . . .	80
5.4	Role of Compression . . . . .	82
5.5	Clinical Applications . . . . .	83
5.6	Shortcomings or Limitations . . . . .	83
<b>6</b>	<b>Conclusion</b>	<b>85</b>
<b>7</b>	<b>Appendix</b>	<b>86</b>
7.1	Matlab Code . . . . .	86
7.1.1	Mullins Effect . . . . .	86
7.1.2	Time Shift . . . . .	86
7.1.3	Filter Analysis . . . . .	87
7.1.4	Fourier Series . . . . .	87
7.1.5	Harmonic Wavelet Analysis . . . . .	87
7.1.6	Wavelet Examination . . . . .	88
7.2	Planes of Dissection . . . . .	89
<b>8</b>	<b>References</b>	<b>90</b>

## List of Tables

1	Brain and Aortic Tissue 40 Cycles at 0% and 33% Compression . . .	39
2	Brain Tissue Time Shift at the End of Each of the First 3 Deformation Cycles . . . . .	46
3	Fourier Coefficients for Frequencies 0-6 Hz of Shear Stress Response (Pa)	58
4	Frequency Ranges for $j$ Levels . . . . .	60
5	Brain Tissue 40 Cycles at 0% Compression (20515a) . . . . .	61
6	Brain Tissue 40 Cycles at 33% Compression (12915a) . . . . .	62
7	Aortic Tissue 40 Cycles at 0% Compression (22515b) . . . . .	63
8	Aortic Tissue 40 Cycles at 33% Compression (22515d) . . . . .	64
9	$L_2$ Error for Binned Wavelets and All Wavelets . . . . .	65
10	Fourier Coefficients for Brain Tissue 0% Compression and 2 Hz . . .	66
11	Harmonic Wavelet Coefficients for Brain Tissue at 0% Compression and 2 Hz . . . . .	67

## List of Figures

1	Phase Shift . . . . .	4
2	Circle of Willis . . . . .	7
3	Clark and Glagov Artery Schematic . . . . .	10
4	Davis Artery Schematic . . . . .	11
5	Dingemans Artery Schematic . . . . .	13
6	Rat Brain Schematic . . . . .	14
7	Illiff Glymphatic System . . . . .	15
8	CSF Circulation . . . . .	16
9	Apparatus . . . . .	20
10	Cleaned Aorta . . . . .	21
11	Skull Diagram . . . . .	22
12	Acoustic Meatus Diagram . . . . .	25
13	Dissection: Rat Brain - Cut 1 . . . . .	26
14	Dissection: Rat Brain - Cut 2 . . . . .	26
15	Rat Brain Specimen . . . . .	26
16	Wavelet . . . . .	32
17	Stress Response of Aortic Tissue under 0% Compression . . . . .	36
18	Stress Response of Aortic Tissue under 33% Compression . . . . .	36
19	Stress Response of Brain Tissue under 0% Compression . . . . .	37
20	Stress Response of Brain Tissue under 33% Compression . . . . .	37
21	Exponential Fit Curve of Aortic Tissue under 0% Compression . . . . .	40
22	Exponential Fit Curve of Aortic Tissue under 33% Compression . . . . .	41
23	Exponential Fit Curve of Brain Tissue under 0% Compression . . . . .	41
24	Exponential Fit Curve of Brain Tissue under 33% Compression . . . . .	42
25	Shoulder on Brain Stress Response . . . . .	43
26	Time Shift for Aortic Tissue Stress Response . . . . .	45
27	Time Shift for Brain Tissue Stress Response under 0% Compression . . . . .	47
28	Time Shift for Brain Tissue Stress Response under 33% Compression . . . . .	47
29	Stress Versus Strain Curve for Aortic Tissue under 0% Compression . . . . .	48
30	Stress Versus Strain Curve for Aortic Tissue under 33% Compression . . . . .	49
31	Stress Versus Strain Curve for Brain Tissue under 0% Compression . . . . .	50
32	Stress Versus Strain Curve for Brain Tissue under 33% Compression . . . . .	50
33	Pass Filter Frequency Decomposition for Brain Tissue Stress Response . . . . .	52
34	Sum of Pass Filter Frequency Decomposition for Brain Tissue Stress Response . . . . .	52
35	Fourier Coefficient Magnitudes: Mover Displacement . . . . .	54
36	Fourier Series Decomposition: Mover Displacement . . . . .	54
37	Fourier Coefficient Magnitudes: Aortic Stress Response . . . . .	56
38	Fourier Series Decomposition: Aortic Stress Response . . . . .	56
39	Fourier Coefficient Magnitudes: Brain Stress Response . . . . .	57
40	Fourier Series Decomposition: Brain Stress Response . . . . .	57
41	Harmonic Wavelet Decomposition Goodness of Fit: Brain, 0% compression . . . . .	59

		vi
42	Harmonic Wavelet Decomposition: Artery, 0% Compression . . . . .	61
43	Harmonic Wavelet Decomposition: Artery, 33% Compression . . . . .	62
44	Harmonic Wavelet Decomposition: Brain, 0% Compression . . . . .	63
45	Harmonic Wavelet Decomposition: Brain, 33% Compression . . . . .	64
46	Harmonic Wavelet Decomposition: Brain, 2 Hz, 0% Compression . . .	66
47	Fourier Series Decomposition: Brain Stress Response, 2 Hz . . . . .	67
48	Axons in Shear Schematic . . . . .	70
49	Positive Shear Direction . . . . .	71
50	Center Shear Direction . . . . .	71
51	Negative Shear Direction . . . . .	71
52	Shear Directions . . . . .	72
53	Damaged Brain Tissue . . . . .	79
54	Planes of Dissection . . . . .	89



# 1 Introduction

Medical information about the mechanical behavior of brain and artery tissues must extend beyond simple characterization of the tissue response to forces to include its correlation with damage since damage in these vital organs can cause life changing effects. Mild traumatic brain injuries result from impacts, high frequency blast waves and inertial acceleration. In the skull, brain matter and arteries lie within close proximity to each other; the Circle of Willis (on the inferior side of the brain) joins several arteries together and branches off to the many smaller arteries that supply oxygen to the cerebrum (Campellone 2015). To better understand brain and aortic tissue's susceptibility to damage, the structures of each tissue, both non-homogeneous biological tissues with high fluid contents, are compared to explore whether the structural differences can explain the differing mechanical response of the two tissues and whether the differing responses may cause damage between the tissues.

In brain tissue research, the mechanics of damage is not well defined. It is hypothesized that the drop in load carrying ability directly correlates to the fluid-solid interaction in the material; the easier the ability for the fluid in the structure to flow (and therefore the more damage that has been inflicted) the more drastic the drop in the load carrying ability. Damage is defined to be a reduction in load carrying capability which may be due to the breaking of bonds within each structure.

The mechanics of an initial insult and repeated loading is of interest not only because many other brain researchers neglect to include the initial impact loading data within their findings, but also because repetitive loadings may cause an increase in damage. Repeated loading does not reduce the carrying ability of aortic tissue in vivo because the aorta undergoes life-long cycles of pressure from blood. The aorta is a natural load bearing material, while brain tissue does not experience regular mechanical insults. The stress responses of brain and aorta tissues in the two materials are speculated to be different due to their difference in structures; however some

response traits should be similar because both tissues have a high fluid content.

The shear stress response to sinusoidal translational shear deformation is used to compare these materials because blood pressure for arterial tissue and shock waves for brain tissue are sinusoidal. Combined compression and shear tests model both the longitudinal and shear component in a deformation wave due to impact for the brain tissue as well as model the combined compression and shear applied to an artery as blood passes through it. The response to repeated loadings in the brain is unknown; however the tissue might not be able to withstand this type of loading without damage.

The goal of this research is to determine how two particular load-bearing and non-load bearing hydrated soft tissues differ in their shear stress response to combined translational shear deformation and unconfined compression. One hypothesis is that a mechanical cause of brain tissue damage under an external mechanical insult is the increased hydrostatic pressure in, and pathological flow of, the extracellular fluid (ECF). A three parameter model is used to fit the peak stress response of bovine aortic tissue and rat brain tissue. Fourier series and harmonic wavelet frequency decompositions are used to analyze the frequencies that exist within the stress response and are related to the structure and fluid in each tissue.

## 2 Background

Aortic tissue and brain tissue are both non-linear viscoelastic materials. Viscoelastic materials are those that exhibit both elastic and viscous properties. These materials behave elastically while loaded quickly but exhibit a continued increase in strain as the stress is held constant called creep. Likewise, viscoelastic materials, when held at a constant deformation after an initial deformation, experience a decrease in stress called stress relaxation. Stress responses of viscoelastic materials are heavily rate dependent due to their viscous properties. The stress response to sinusoidal deformation may be sinusoidal or quasi-periodic, oscillations that may follow a regular pattern but do not have a fixed period. A sinusoidal shear stress response may exhibit a phase shift compared to the deformation which may depend on amplitude, frequency and damping. If the response is quasiperiodic, the time shift may also depend on these factors and may change with the number of cycles. The dependence for linear elastic materials can give guidance in assessing the influence of these factors for both brain and aortic tissue. The damping factor may be related to the role of the interstitial fluid which may be responsible for the viscoelastic response in both tissues.

### 2.1 Phase shift

Linear viscoelastic materials subject to an oscillatory strain input respond with a stress having the same frequency as the strain, however the curves are not synchronized in time. The difference in synchronization can be characterized by the phase shift. The phase shift is the difference in time between the displacement and stress sine waves as they cross through the horizontal axis measured with respect to a corresponding cycle in radians or degrees. A phase shift can be measured only when both a sinusoidal strain input versus time curve and a force versus time curve exhibit the same frequency response. The phase angle,  $\delta$ , numerically describes the lead or

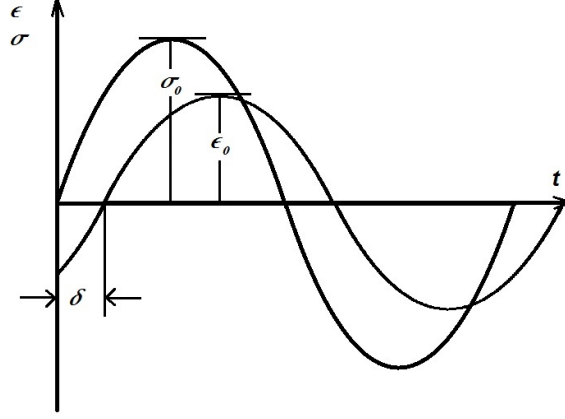


Figure 1: Stress and strain curves having the same frequency but different amplitudes, for which stress leads strain by  $\delta$ .

lag that one curve has compared to the other; a curve leads if its corresponding cycle crosses the horizontal axis at an earlier time. The phase angle can also be calculated as a time shift given as

$$\Delta t = \frac{\delta}{2\pi f} \quad (1)$$

where  $f$  is the frequency.

The experimentally determined phase shift should give information about the viscosity of the tissue. The following simple examples give insight into the possible relation between phase shift and bulk viscosity. The sinusoidal stress and strain for a strain input are

$$\epsilon = \epsilon_0 \sin(\omega t); \quad (2)$$

$$\sigma = \sigma_0 \sin(\omega t + \delta); \quad (3)$$

where  $\delta$  is the phase shift, also called the phase angle. The storage modulus  $E_1$  and the loss modulus  $E_2$  are

$$E_1 = \frac{\sigma_0}{\epsilon_0} \cos(\delta); \quad (4)$$

$$E_2 = \frac{\sigma_0}{\epsilon_0} \sin(\delta). \quad (5)$$

The tangent of the phase angle  $\delta$  is calculated by taking the ratio of the loss modulus

and the storage modulus,

$$\tan(\delta) = \frac{E_2}{E_1}. \quad (6)$$

In linear viscoelasticity, dynamic mechanical analysis characterizes the phase shift observed during oscillatory testing by relating the energy stored to the energy lost. The dynamic modulus of a material is the complex sum of the storage modulus and the loss modulus. The tangent of the phase shift is the ratio of the elastic and dissipative energies (or the storage and loss moduli)(Equation 6), therefore, if no energy is lost or if the material is purely elastic, the phase shift is zero. A material that is purely viscous, on the other hand, would only have energy lost and would have a phase shift of  $90^\circ$ .

The Standard Solid model, a spring ( $R_1$ ) connected in parallel with Maxwell's model (a spring ( $R_2$ ) and dashpot in series), demonstrates the behavior of a linear viscoelastic material. This standard linear solid model is

$$\dot{\epsilon} = \frac{R_1}{\eta} \left( \frac{\eta}{R_2} \dot{\sigma} + \sigma - R_1 \epsilon \right). \quad (7)$$

For sinusoidal strain control,  $\epsilon = \epsilon_0 \sin(\omega t)$  is substituted into this equation to yield

$$\omega \epsilon_0 \cos \omega t = \frac{R_1}{\eta} \left( \frac{\eta}{R_2} \dot{\sigma} + \sigma - R_1 \epsilon_0 \sin \omega t \right). \quad (8)$$

The differential equation solved to obtain stress is

$$\begin{aligned} \sigma(\omega t + \delta) &= \frac{1}{R_1(R_2^2 + \eta^2\omega^2)} \epsilon_0 R_2 [e^{-\frac{R_2 t}{\eta}} \eta \omega (R_1^2 - R_1 R_2 - R_2^2) \\ &\quad - \eta \omega (R_1^2 - R_1 R_2 - R_2^2) \cos \omega t \\ &\quad + (R_1^2 R_2 + \eta^2 R_1 \omega^2 + \eta^2 R_2 \omega^2) \sin \omega t] \end{aligned} \quad (9)$$

Use the sum of sines to obtain

$$\tan(\delta) = \frac{\eta(-R_1^2 + R_1R_2 + R_2^2)\omega}{R_1^2R_2 + \eta^2R_1\omega^2 + \eta^2R_2\omega^2}. \quad (10)$$

If the spring in series with the dashpot ( $R_2$ ) is larger than the stiffness of the spring in parallel ( $R_1$ ) the tangent will be positive which means that the stress leads the strain. If the opposite stiffness is true ( $R_1 > R_2$ ), the strain leads the stress.

The Zener standard solid model (used by Dennerll et al. (1989) to model an axon in tension), a spring ( $R_2$ ) connected in series with a Kelvin-Voigt model (a spring ( $R_1$ ) in parallel with a dashpot) is

$$\sigma + \frac{R_1}{R_2}\sigma + \frac{\eta}{R_2}\dot{\sigma} = R_1\epsilon + \eta\dot{\epsilon}. \quad (11)$$

Under sinusoidal displacement control,  $\epsilon = \sin(\omega t)$  is substituted into this equation to produce

$$\left(1 + \frac{R_1}{R_2}\right)\sigma + \frac{\eta}{R_2}\dot{\sigma} = R_1 \sin(\omega t) + \eta\omega \cos(\omega t). \quad (12)$$

Solve the differential equation to obtain the stress

$$\sigma(\omega t + \delta) = \frac{R_2(-e^{-\frac{(R_1+R_2)t}{\eta}} R_2\eta\omega + R_2\eta\omega \cos(\omega t) + (R_1^2 + R_1R_2 + \eta^2\omega^2) \sin(\omega t))}{R_1^2 + 2R_1R_2 + R_2^2 + \eta^2\omega^2}. \quad (13)$$

Use the sum of sines to obtain

$$\tan(\delta) = \frac{R_2\eta\omega}{R_1^2 + R_1R_2 + \eta^2\omega^2}. \quad (14)$$

The tangent of the phase angle in the Zener model is always positive, meaning that stress leads strain. Although the Zener and Standard solid models cannot capture the complexity of heterogeneous biological tissue, these models demonstrate the dependence of phase shift on  $\omega$  and the material parameters. The non-linearity of

the biological tissue stress response may cause a phase shift that depends on other factors than the linear model variables. These dependencies guide the investigation into the cause of any time shift in the brain and aorta shear stress response.

## 2.2 Tissue Structure

Several arteries lie within close proximity to the brain including the Circle of Willis, a joining area on the inferior side of the brain that branches into small arteries that carry oxygen to 80% of the cerebrum (Campellone 2015). Arterial tissue and brain tissue, although both soft biological tissues with high fluid content, have different physical requirements. Arteries naturally expand and contract as blood pulses which causes a compressive stress in the radial direction, a tensile stress in the circumferential direction, and shear stresses. The effect of shear is of interest because it has not been studied in much detail. Brain tissue undergoes a combined compressive and shear stress wave during a blast. A comparison of the response to combined compression and shear for both the brain and artery should be informed by an analysis of the structures of each material.

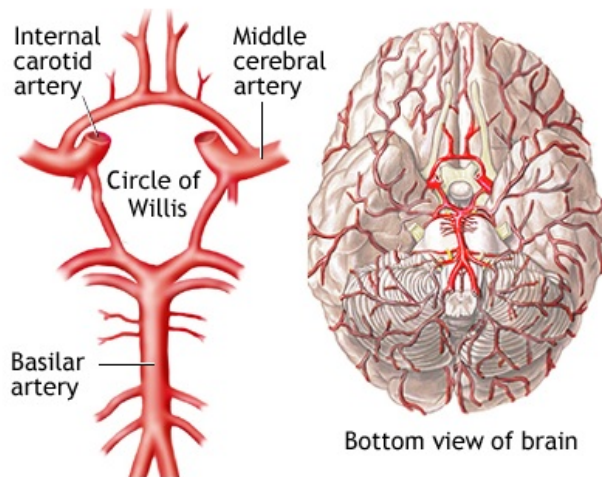


Figure 2: Circle of Willis (Campellone 2015)

### 2.2.1 Artery

Arterial tissue is a natural load bearing, soft biological tissue with high interstitial fluid content and is comprised of three main layers called the intima (inner), media (middle) and adventitia (outer). The intima is composed of endothelial cells, connective tissue and axially oriented smooth muscle cells with an underlying layer of collagen fibers. Ground matter is situated on either side of these fibers parallel to the intimal and adventitial faces. Histology has shown a dominant direction of collagen fibers in the circumferential direction with local variation. The internal elastic lamina which separates the intimal and medial layers is comprised of an elastin sheet that is responsible for transporting fluid. The media is comprised of many smooth muscle cells, elastin and collagen (Figure 3). The fluid is located in the smooth muscle cells and in the extracellular matrix (ECM). The extracellular fluid (ECF) is responsible for transporting nutrients to the cells. Versican proteoglycans are the main filler substance in between cells which bond to water and allow for diffusion of nutrients to the cells. These proteoglycans form large complexes and attach to collagen to regulate the movement of molecules through the arterial wall.

Three schematic models are proposed in the literature for the structural organization of the aortic wall. These models eventually may allow an assessment of the corresponding effects each set of substructures would have on the mechanical response.

Clark and Glagov (1985) proposed from histology images that the arterial wall is comprised of overlapping, musculo-elastic fascicles which consist of smooth muscle cells, elastin sheets, and collagen fibers which are similarly oriented. The commonly oriented smooth muscle cells are encompassed by a matrix mat comprised of a fine mesh-work of collagen fibrils. This matrix is related to a “Chinese finger trap” in Clark and Glagov (1979), stating that the matrix holds the cells together when tension forces exist. These fascicles were observed to be anchored by elastic fibers and in the media lie mainly circumferentially. Wavy collagen bundles that never interfere



with one another are oriented in the same direction as nearby elastin forms sheets. Clark and Glagov note that there were connections between elastin fibers of each layer that are “more easily disrupted than the elastin systems bracketing the layers.” They argue that the medial wall is comprised of a repeating sequence of “elastin-cells-elastin - collagen bundles - elastin- cells- elastin” (Figure 3). While the fascicles are predominately oriented in the circumferential direction in the media, Clark and Glagov found that the fascicles favor an axial orientation in the adventitia and luminal side. Clark and Glagov conclude that there exists distinctly aligned collagen and elastin on both sides of a cell layer. This predominately circumferential oriented fascicle direction theory would create a mechanical response that hardens because the matrix mat would create an increase in strength as a circumferential tensile force is exerted. This theory implies a significant difference in shear response with respect to specimen orientation, when deformed with or across the specimen fiber direction.

Using Clark and Glagov’s schematic model, when the tissue experiences a shear force the longitudinally oriented specimens would predominantly test the connections between the wall layers and the connections between the fascicles. The circumferentially oriented specimens would predominantly test the strength of the collagen fibers in shear. Both oriented specimens could test the strength of the interfiber bonds between collagen fibers (Haslach et al. 2015b).

Much like the observations of Clark and Glagov, Davis (1993) reported that in the aortic media there exists circumferentially oriented smooth muscle cell layers alternating with elastic laminae (Figure 4). Davis observed that smooth muscle cells are connected to the elastic laminae (which Davis refers to as musculo-elastic units) within the aortic wall in alternating diagonal patterns. Davis boldly hypothesizes that the tangential vessel wall stresses are not affected during regular blood pressure induced deformation. Davis observed that a single elastic lamina separates each smooth muscle cell layer in mice which differs from the double elastic laminae found

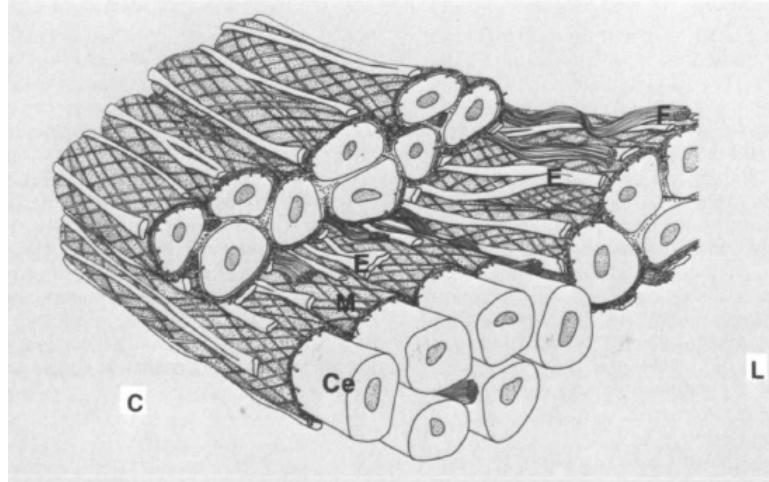


Figure 3: Clark and Glagov Artery Schematic (C indicates the circumferential plane, L indicates the longitudinal plane) Each musculo-elastic fascicle contains commonly oriented cells (Ce) enclosed in a matrix mat (M) surrounded by a system of elastic fibers (E) and wavy collagen bundles (F). (Clark and Glagov 1985)

in larger mammals' aortic walls as described by Clark and Glagov. Davis mentions the findings of Pease and Paule (1960) that describe smooth muscle cell layers of the rat aortic media as a single layer of obliquely oriented cells with each cell extending from one elastic lamina to the next, the orientation of the smooth muscle cells changing direction in successive layers. This herringbone design theory creates a different mechanical response than the Clark and Glagov model.

Davis' herringbone schematic design (Figure 4) implies that the tissue would experience a tensile force within the contractile-elastic units when a longitudinal shear stress is applied; the angled contractile-elastic units would be stretched out of the circumferential plane. The response due to pure circumferential tension creates internal shearing between the elastin layers due to the alternating contractile-elastic units. The mechanical response due to shear would create a tensile stress within the contractile-elastic units oriented in one direction and would create a shear stress in the smooth muscle cells in the layers with opposing contractile-elastic unit direction.

Much like Davis' discussion of musculo-elastic units, Dingemans et al. (2000) discusses a similar basic unit of the aortic media, the lamellar unit, which consists

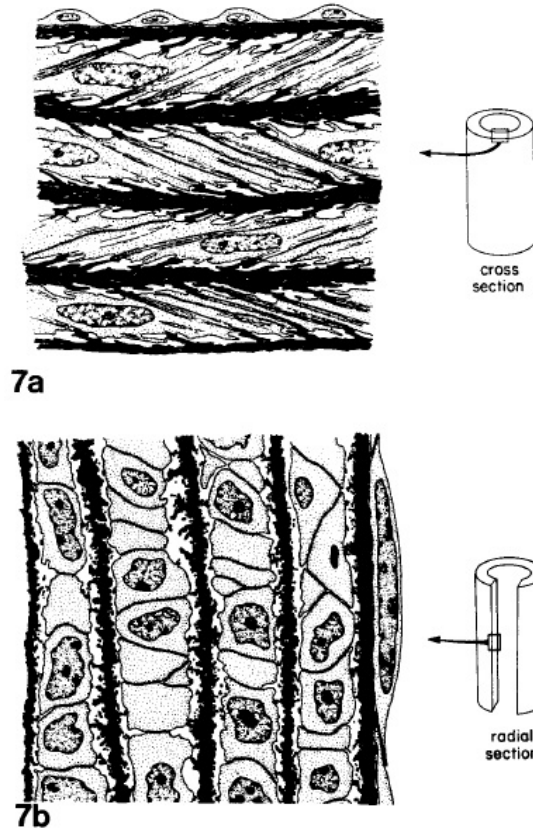


Figure 4: Davis Artery Schematic (Davis 1993)

of two elastic lamellae and intervening smooth muscle cells. These lamellar units are comprised of a single layer of smooth muscle cells with elastic lamellae on both sides (Figure 5). Dingemans noted that in collapsed specimens there exists wavy elastin lamellae and that while parts of the lamellae were smooth, there were also irregular focal protrusions that extended into the interlamellar space. The Dingemans model agrees with Clark and Glagov (1985) in that the smooth muscle cells are oriented mainly in the circumferential direction. Dingemans et al. observed that there are relatively few direct contacts of smooth muscle cells with solid elastin lamellae and that the smooth muscle cell extensions were found in close contact with irregular protrusions from the elastin lamellae. Dingemans makes a contrasting argument to Clark and Glagov's "Chinese finger trap" theory of collagen fibril net organization that preferential localization of collagen fibrils immediately adjacent to the smooth

muscle cell surface was not observed. Dingemans et al. interpret their images as showing that the collagen fibrils appear loosened and spiraled. Dingemans et al. state that they did not observe any organization of the aortic medial in ‘musculo-elastic fascicles’ as described by Clark and Glagov (1985) in several non-human species.

Dingemans et al. describe the structure of the aortic wall saying the longitudinal surface ridges of the smooth muscle cells are connected by long elastin protrusions to the lamellae on either side. The smooth muscle cells are also connected with the elastin lamellae via oxytalan fibers that contain collagen. The collagen fiber bundles are described to lie directly against the elastin lamellae in the circumferential direction. The fibronectin appeared to not only connect smooth muscle cells to the elastin sheets, but also to each other. Dingemans et al. observe that the smooth muscle cells were connected by numerous gap junctions. Dingemans et al. conclude that the collagen fibrils located adjacent to the smooth muscle cell surface as noted in Clark and Glagov (1985), were absent.

Dingemans structural theory would create a mechanical response that would primarily test the tensile strength of the elastin protrusions and after some displacement, the smooth muscle cells and the oxytalan fibers that link them to the elastin sheets would also be in shear and tension respectively. The linking elastin protrusions exhibit different directions that would correlate to a lack of a significant difference between the tested specimen orientations within small shear deformation; Dingemans theory of predominately circumferential collagen fibers would affect the mechanical response after the fibers become taut. Holzapfel et al. (2000) assume this mechanical response within their mathematical models.

Dingemans et al. note the proteoglycans that surround all collagen fibrils are oriented perpendicularly to the fibril direction. The ground substance appears completely filled with large proteoglycans seen on the very cell surface, but the elastin lamellae and the oxytalan fibers do not contain proteoglycans. The location of pro-

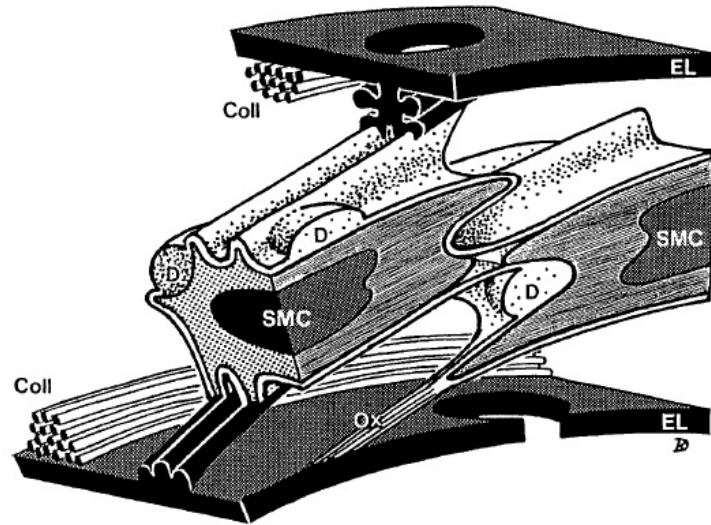


Figure 5: Dingemans Artery Schematic. The schematic shows smooth muscle cells (SMC) and elastin lamellae (EL) and their connections. The collagen fibers (Coll) lie closely to the elastin lamellae. Oxytalan fibers (Ox) connect the elastin lamellae to the smooth muscle cells. Deposits (D) of collagen and proteoglycans are found on the cell surface. (Dingemans 2000)

teoglycans can indicate the primary locations of extra-cellular fluid within the tissue.

The collagen fibers act as a restraint to deformation. When the artery tissue is relaxed, the collagen fibers are slack and when the tissue expands due to blood pressure, the elastin sheets stretch and the collagen fibers become taut, restraining the tissue.

Haskett et al. (2010) discuss probable cross-linking that bond between circumferentially oriented bands of collagen fibers. This theory was drawn from tensile testing performed perpendicular to the primary collagen fiber direction that results in a higher stiffness than the tests performed in the direction of the collagen fibers.

### 2.2.2 Rat Brain

Brain tissue is a heterogeneous soft biological tissue comprised of many subsections of both white and grey matter and is not a natural load bearing material (Figure 6). Brain tissue solid matter is primarily neurons and glial cells. A neuron is a

nerve cell that transmits information through electrical and chemical signals. The axons of the neuronal cells are responsible for carrying the electrical impulses from the cell body toward the axon terminal to send information to other axon dendrites which creates a network of neurons. Brain tissue has both a high intra- and extracellular fluid content of around 80% of its mass. Extracellular fluid (ECF) which makes up 20% (Verkman 2013) of the brain's volume is responsible for transporting nutrients from the capillaries to the cells and for removing waste from the cells as part of the glymphatic system. The ECF creates an internal pressure in the brain that is balanced by a linked network of axons in tension. Brain tissue does not have a structured framework supporting the tissue as does the artery. The balance between the internal pressure of the ECF and the tension within the axons allows the tissue to keep its shape, and neurites adjust their length accordingly to maintain a steady tension (Van Essen 1997). Brain tissue has viscoelastic properties and is under resting tension which is demonstrated by the tissue's ability to spring back to its original position after a transient deformation. Van Essen states that all cells have a natural pressure differential across their plasma membrane, resulting from a mechanism to regulate the osmotic balance, but pressure can also arise from extrinsic sources.

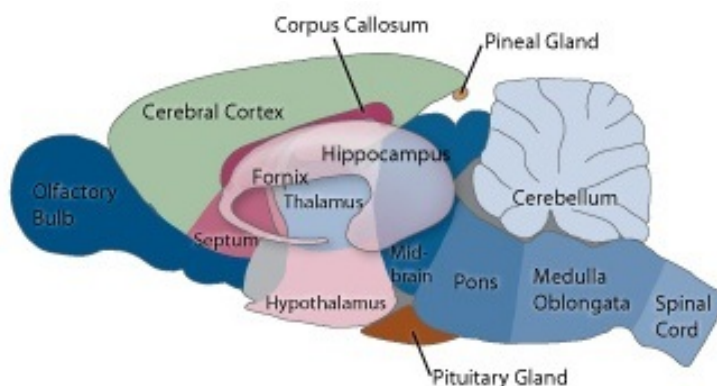


Figure 6: Rat Brain Schematic (University of Utah Health Sciences 2015)

Astrocytes are star-shaped glial cells that provide biochemical support of the blood-brain barrier, provide nutrients to the nervous tissue, maintain the extracellular ion balance, and repair/scar the brain after traumatic injury. Three types of astrocytes are involved in the physical structuring of the brain. Fibrous astrocytes that are located in white matter that are responsible for connecting the cells to the outside of capillary walls, protoplasmic astrocytes are located in grey matter and radial astrocytes are present during childhood development. Glial cells provide support for the neurons to protect the brain. These cells also supply the neurons with nutrients and oxygen because neurons are very active and generate a lot of waste. The process of fluid redistribution, nutrient transport and waste removal within the brain is referred to as the glymphatic system. Cerebrospinal fluid (CSF) is generated in the 4 ventricles of the brain and moves through the subarachnoid compartment (Figure 8). Iliff et al. (2012) describe the flow path of CSF and interstitial fluid (ISF) as driven by the pulsing arteries in the brain that cause a pressure change between the para-arterial and paravenous pathways (Figure 7).

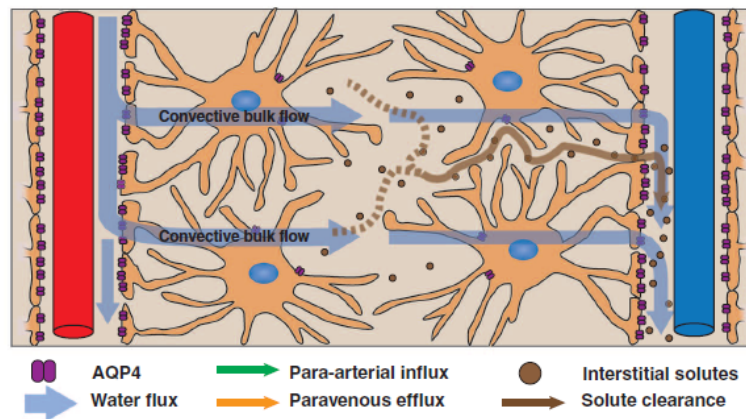


Figure 7: Fluid flow in glymphatic system (Iliff 2012)

Iliff et al. propose that channels between cells provide low-resistance pathways for fluid movement between the paravascular spaces. Due to the gaps between the astrocytes endfeet in the astroglial sheath that surround brain blood vessels (Mathiisen et al. 2010), the nutrient filled fluid is able to flow between the dendrites, but that the

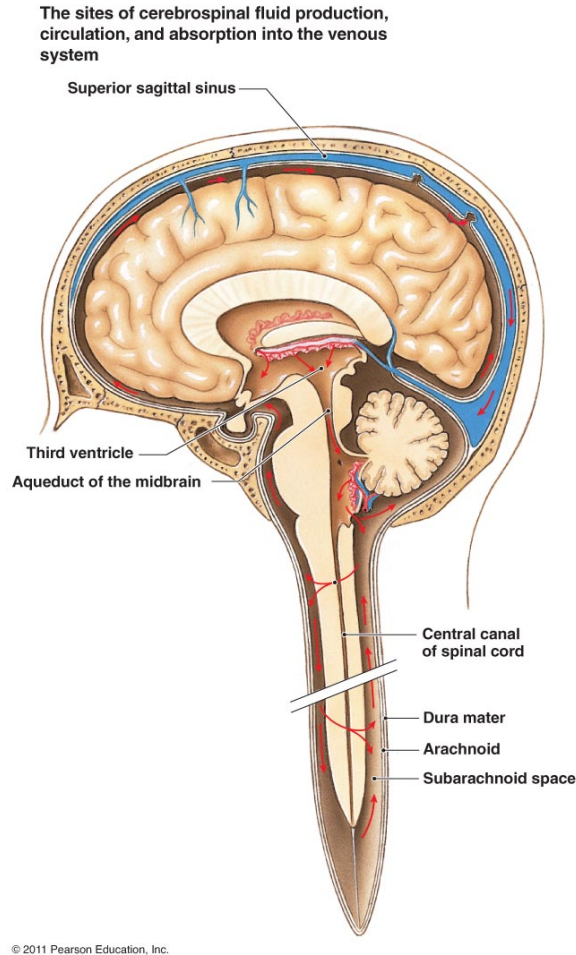


Figure 8: CSF Circulation in humans (Silverthorn 2011)

exchange of fluid between the blood and brain is controlled by the size of the narrow clefts between overlapping endfeet of the astrocytes which may restrict free flow of the fluid. The CSF distributes the nutrients to the cells and picks up the metabolites in the process and continues flowing toward the veins. The veins reabsorb the waste and carry it to the cervical lymphatic system.

Damage within the brain can be categorized into two types: cell damage and structural damage. Structural damage consists of the breaking of axonal connections and may result in a separation of subregions. Structural damage could also include the stretching of the axons. A strain of 20% has been suggested as the threshold for diffuse axonal injuries (Bain and Meaney 2000). An increase in hydrostatic pressure



causes stretching or relocation of subregions. Cell damage consists of the rupture of cells or change in the cells' permeability due to stretching of the cell walls.

Unconfined compression tests (Haslach et al. 2015) provide information about the ECF-solid phase interaction in which the ECF-flow is multi-axial. A constant deformation rate compression causes a disruption in the brain tissue's equilibrium balance of hydrostatic pressure. The lateral dimension changes indicates that the tissue is compressible due to ECF loss. The tissue's interstitial fluid may move in all directions within the tissue causing transverse stress due to the drag force between the fluid and solid phase. The compression may induce axonal stretching. The solid matter's resistance of ECF flow could be caused by the further restriction of extracellular space in the compressed tissue.

### **2.3 Mullins Effect**

In cyclic tensile tests, some biological tissues exhibit stress softening (Horney et al. 2010). This phenomenon is referred to as Mullins effect. Diani et al. (2009) observed that in rubber most of the softening appears after the first load. This softening occurs whenever the strain of the current cycle is less than or equal to the maximum stretch ever applied. The physical explanation of Mullins effect has not been generally agreed upon, but may be due to chain breakage, slipping of molecules, and cross-link ruptures. Blanchard and Parkinson (1952) as well as Bueche (1960) attribute the Mullins effect to bond rupture and crosslinking. Diani et al. describes the Mullins effect to be due to the rupture of carbon-black structure in rubber. Typically, on the initially loading, the material exhibits a relatively stiff response. When the material is unloaded and then reloaded the stress-strain curve softens significantly. Zuniga and Beatty (2002) describe the material as having a selective memory of only the maximum of the previous strains ever experienced and represent the Mullins effect with a 3 parameter model to fit the exponential type stress softening (Equation 15),

$$F(m, M) = \exp(-b\sqrt{M - m}) \quad (15)$$

where  $M$  is the maximum previous strain,  $m$  is the current magnitude of strain, and  $b$  is a softening parameter.

Mars et al. (2004) observes that the steady state of the response due to torsional applied shear is softer if larger initial magnitudes of strain are experienced. They discovered that the majority of the softening occurred in the first 10 cycles of loading and that under constant-amplitude cyclic loading the stress-strain curve exhibits a logarithmic trend. In some cases, Mars et al. describe without explanation a new phenomenon called the ‘healing’ effect in which after several cycles, the stress-strain response remains relatively constant and then starts to slightly stiffen.

## 3 Methods

Arterial and brain tissue can experience internal deformation waves which consist of both longitudinal and shear components simultaneously (translational shear and compressive waves). Aortic and brain tissue are tested in an apparatus that can operate in translational shear with an initial fixed unconfined compression.

### 3.1 Apparatus

The apparatus (Figure 9) was constructed to test cut rectangular specimens of dimensions up to 25 mm x 25 mm with thicknesses up to 8 mm in shear. The specimen is placed between two parallel test plates. The bottom plate (9 -10) is mounted to a Bose 250 gram load cell (Figure 9 -3) and rests on top of a linear bearing (Figure 9-1). The linear bearing ensures that the bottom test plate remains flat and parallel to the top plate with negligible friction detected by the load cell. The other end of the load cell is secured to a support bracket (Figure 9-8). This support is essential to the design because one end of the load cell must be fixed at all times in order to deflect due to the applied forces. The support bracket is connected to a spring-loaded displacement stage, ThorLabs T12X (Figure 9-9), that enables the bottom plate and load cell to move up and down as a unit to increase or decrease the compression on the specimen and to adjust for different specimen thicknesses. This assembly is fastened to a mounting bracket (Figure 9-4) that is screwed into a stationary stand. The top test plate (Figure 9-11) is mounted on a Bose Electroforce Test Bench 200 N test machine that uses a linear motor design that is modified from a Bose sub-woofer. The Bose machine is composed of a permanent magnet that is suspended in an electromagnetic field. The magnet is able to produce translational motion as the electromagnetic field changes. This design reduces any frictional energy loss by avoiding the use of bearings or seals. The oscillating magnet is attached to an ac-

tuator to record any error that occurs. The Bose machine allows the top test plate to move linearly or sinusoidally at a set rate up to 3.2 m/s or 200 Hz and to a set final displacement (Chan et al. 2008). The Bose proprietary software, WinTest 4.1, is used to appropriately assign each variable for a given test.

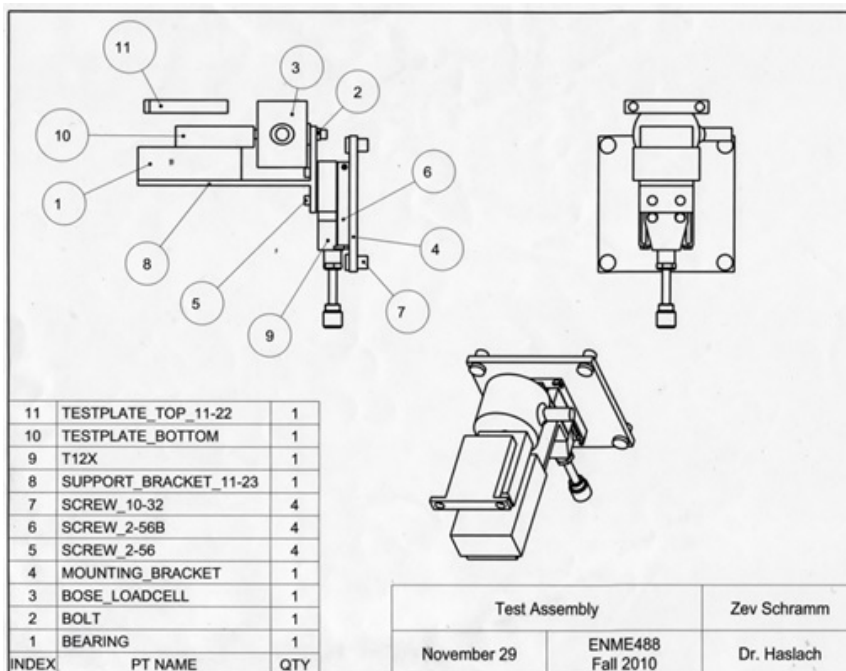


Figure 9: Combined translational shear and unconfined compression apparatus

## 3.2 Specimen Preparation

Specimens are cut from bovine aortic tissue and from rat brain tissue.

### 3.2.1 Aorta

The samples are taken from bovine descending aorta purchased at J. W. Treuth & Sons (328 Oelle Ave. Baltimore, MD 21228). The aorta must first be cleaned of fat before the samples are taken from it; excess branches from the aorta as well as any additional portions of the heart are removed with a No. 10 blade scalpel (Figure 10). Because the curvature of the aorta is very sharp at the proximal end of the aorta,

this section is removed.



Figure 10: Cleaned bovine aorta

Once this process is completed, a ring is cut from a location of the tester's choice that is approximately 6+ mm in width. The thickness of the sample varies by location on the aorta. For our tests, the specimen is cut from the middle section of the aorta. After the ring is cut open by making a longitudinal incision along the convex side, a tensile pattern fixture is used to cut the open ring along the circumferential direction to create a strip with a width and length of approximately 6mm. Blue dye is used to mark one of the two circumferential sides of each rectangular specimen so the tester can record whether the specimen is loaded in the circumferential or longitudinal direction.

### 3.2.2 Brain

The brain must be removed without damage by the carefully executed following procedure. (See Appendix, Section 7 for Planes of Dissection, Figure 54).

Place the euthanized rat dorsal surface up on a surgical mat with the anterior side facing up. Using surgical scissors and tissue forceps, pinch the skin on the dorsal surface by the nape of the neck and make a longitudinal incision at the mid-line. Insert one end of the scissor blades under the skin surface to further the incision longitudinally to the right and left side of the upper neck. With a No. 11 blade

scalpel make transverse cuts into the muscle tissue just below the base of the skull, using the forceps to separate the tissue as the cuts become more medial. Once the muscle is separated on the posterior and lateral sides of the neck, open the hand held bone cutters (Fine Science Tools #16107 – 14) slightly so that the opening of the curved jaws can fit the width of the spine. Holding the bone cutters vertically, insert the jaws of the cutters on either side of the spine where the muscle tissue was separated slightly distal to the skull and deep enough to ensure the length of the jaws go slightly further than the depth of the spine. Slowly grip the bone cutters to cut through the spine. Once the bone has separated, use the scalpel to cut the remaining connecting tissue to complete the decapitation.

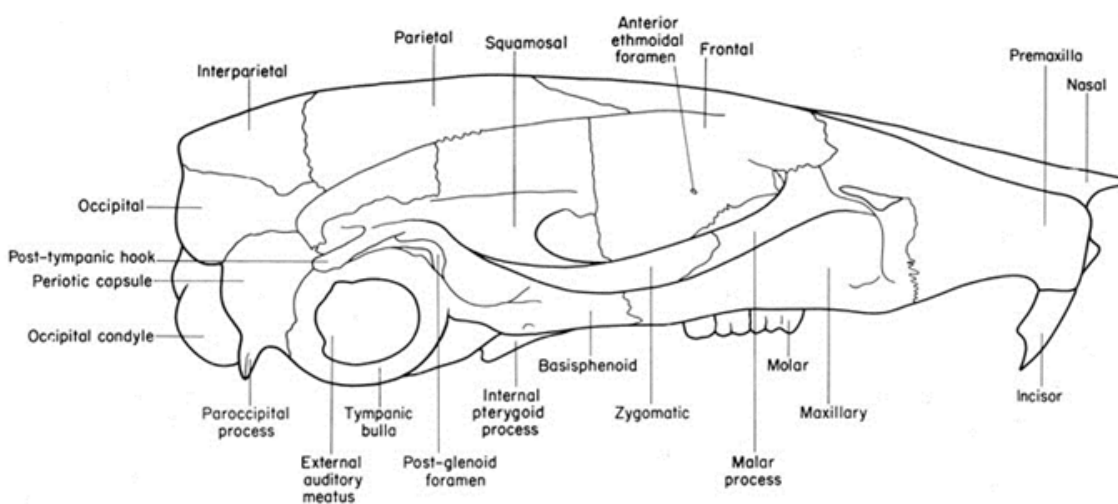


Figure 11: Mouse Skull Diagram (The Jackson Laboratory 2015)

After decapitation, make a sagittal incision down the center line of the head from between the eyes back to the furthest posterior position. By pulling and if needed making swift superficial cuts along the medial of the skin, separate the skin from the muscle tissue on both the right and left sides to expose the muscles on the sides of the skull.

Holding the head in the non-dominant hand and using the bone cutters in the dominant hand, grab, twist slightly and pull the muscle tissue from the posterior

occipital in jaw-sized pieces (Figure 11). When most of the muscle tissue is cleared from the occipital, rest the right side jaw of the bone cutters with the blade proximal to the skull on the superior edge of the occipital and while grasping the handles of the bone cutters allow the left side jaw to gently scrape against the bone to remove the residual muscle tissue. If any cerebral disks are still connected to the skull, gently insert one jaw of the bone cutters from the posterior side through the hole of the disk along the dorsal surface without coming in contact with the spinal cord and make the cut. Grab the side of the cut disk that agrees with the researcher's dominant side and twist and pull toward the distal direction. Once all of the disks have been removed, insert the bone cutters from the posterior side through the occipital hole, being very careful not to come in contact with the brain tissue with the rounded edge of the bone cutters facing medially and the sharp edge of the jaw placed inside of the skull riding the inner surface of the occipital so that the tip of the jaw blade points toward the dorsal, lateral corner of the occipital. Cut the occipital at this angle on both the right and left sides (making sure that the rounded edge of the bone cutters is facing the medial direction for both). Putting the bone cutters in the sagittal plane with the rounded edge of the bone cutters facing toward the occipital, insert the lower cutter jaw under the flap of the occipital that was created from the angled cuts. Lean the upper jaw on the back of the interparietal and while keeping the upper jaw of the bone cutters stable (like a joint), rotate the occipital flap away from the brain (in the posterior and dorsal direction). The dorsal surface of the skull has two visible ridges running in the sagittal plane on either side of the skull (these ridges exist at the most medial intersection of the muscle tissue on either side of the skull and the bone).

With the curved edge of the bone cutters facing the medial direction, and directed in the sagittal plane pointing toward the rostral direction (toward the nose) make small cuts along the ridge on either side of the skull. Once cuts of approximately 1-3 mm have been made on both sides, the same approach can be used to remove this

flap as was used to remove the occipital flap. Work down either side of the ridges until the brain is exposed and the ridges begin to curve in the medial direction.

The dura mater should still be intact at this point, but must be removed so the brain is unrestrained. Along the interface of the left and right hemisphere of the cerebrum, a dark red line should be visible. Using the tip of the bone cutters, lightly grab this line and pull very gently away from the surface of the brain and snip the connection. The same should be done along the interface between the cerebellum and the cerebrum.

Now the top of the brain should be fully exposed, however there are still bones that are holding the brain in place that lie between the interface of the cerebrum and cerebellum. The external acoustic meatus can be seen pulled from the interface of the cerebrum and cerebellum (Figure 12). Bring the bone cutters in the coronal plane, with the rounded edges facing the table toward the posterior side of the skull. By tilting the bone cutters so the rounded edge faces toward the medial direction slightly, insert the more medial directed jaw along the intimal surface of the side wall of the skull at a depth of approximately 4 mm. Clamp the bone cutters slightly enough to grab, but not cut, and twist along the lateral-medial axis in the lateral direction. If the bone cutters are clamped too tightly, the bone will snap while twisting. This process should be repeated on the other side. The twisting action ensures that the acoustic meatus, which restrains the brain from being lifted from the skull, is removed and does not damage the brain tissue in the process of its removal.

Remove the brain from the skull by flipping the skull upside down over a small tray filled with PBS. Insert a surgical elevator between the ventral side of the brain and the skull and gently assist the falling process of the brain into the tray. Small cuts will need to be made to the olfactory bulbs and to any other connecting tissues from the brain to the base of the skull. Allow the brain to fall into the tray being sure that the brain is not pushed on by the elevator. This concludes the process of



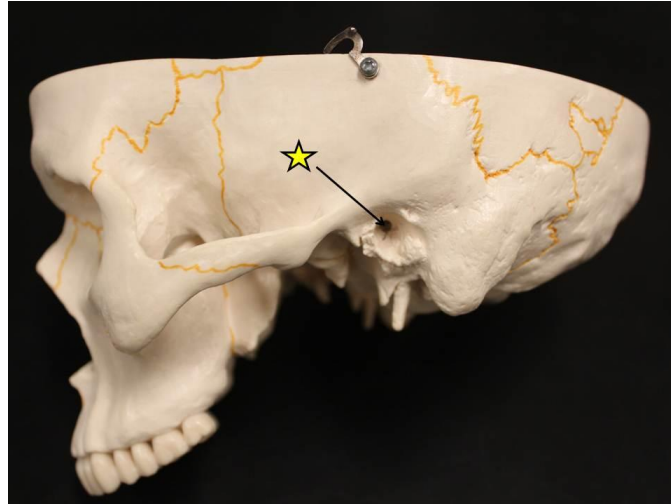


Figure 12: External acoustic meatus on human skull (Seward 2015)

harvesting a rat brain without damaging the tissue prior to testing.

After excising the brain from the rat, an incision is made with a No. 11 blade scalpel parallel to the frontal plane to separate the cerebellum from the cerebrum (Figure 13). A surgical elevator is moistened in the PBS to create a thin film of fluid on the tool. The fluid creates a barrier to ensure that the brain tissue does not stick to the tool. The surgical elevator is used to gently lift the cerebellum to place it into a tray of PBS to avoid dehydration of the specimen. An incision is then made down the center line of the cerebrum to separate its two halves (Figure 14). The separation of the two cerebrum halves requires multiple stabbing cuts directed straight down rather than a sawing or pivoting blade cut which could damage the tissue.

Each cerebrum half is cut in the sagittal plane into 3 mm thick specimen; creating two specimens from each half (Figure 15). These specimens are lifted with a surgical elevator into the PBS as well. The sagittal plane specimens are trimmed to 12 mm x 6 mm to ensure consistency throughout the tests. When it is time to test a specimen, the surgical elevator is again moistened and then used to scoop each specimen out of the tray filled with PBS. Using a surgical elevator is ideal, opposed to using tweezers or other devices, because the specimen is not squeezed, merely lifted. A total of 24

(12 rat brain specimens and 12 aortic) were tested.



Figure 13: Post cerebrum removal



Figure 14: Post cerebellum separation

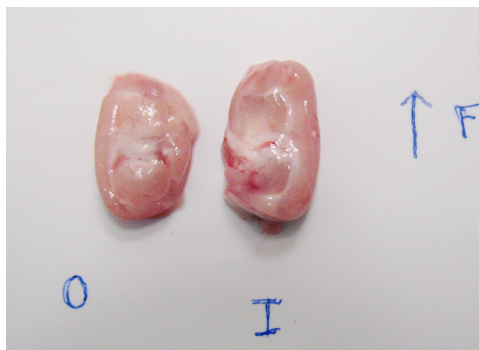


Figure 15: The left half of the cerebellum cut to make 2 specimens. The incision plane is facing upward for both specimens showing the heterogeneity. (O indicates the outermost specimen, I indicates the inner specimen and the arrow pointing toward the front side of the brain.)

### 3.3 Protocol

To begin testing, the Bose stationary stand is loosened from the base and moved away from the top grip. By doing this, the researcher has more room to carefully place a drop of 3M VetBond No. 1469SB glue on the bottom plate to secure the specimen. The specimen can easily be slid off the moistened surgical elevator and must be precisely placed in its desired alignment on the bottom grip (with the 6 mm side facing the Bose and the 12 mm side for the brain tissue facing perpendicular to the Bose and with the circumferential direction parallel to the mover's direction for the aortic tissue). The specimen cannot be moved once placed without damaging the tissue because the glue dries quickly. Another drop of glue is placed on the top of the specimen. While one hand holds the spring loaded T12X in its lowest position, the stationary stand is readjusted to a position in which the top and bottom plate realign. Holding the plate down is essential to avoid additional normal loading on the specimen. The stationary stand is refastened and the bottom plate is released slowly upwards. The T12X is adjusted to raise the bottom plate so that the specimen is squeezed to the desired thickness.

Throughout the test, WinTest 4.1 records the elapsed time, displacement, and the reactive load induced in the load cell. The scan time is set to the fastest programmable time of 0.0002 seconds to maximize the number of points during a test. Translational shear stress is calculated from the detected load from the bottom grip of the apparatus (Figure 9) by

$$\sigma = 10^{-3} \frac{g\mathcal{F}}{\mathcal{A}} \quad (16)$$

where  $g$  is the gravitational constant,  $\mathcal{F}$  is the detected load (in grams), and  $\mathcal{A}$  is the cross sectional area parallel to the test plate (in  $m^2$ ). The translational shear strain

is calculated from the detected displacement of the mover by

$$\epsilon = \frac{d}{L} \quad (17)$$

where  $d$  is the detected displacement (in mm) and  $L$  is the length of the specimen (in mm) in the direction parallel to the displacement direction.

### 3.3.1 Combined Sinusoidal Translational Shear and Fixed Initial Unconfined Compression

Aortic tissue experiences sinusoidal shear stresses due to blood pressure oscillations; likewise, brain tissue can experience sinusoidal shear due to a blast wave. An unconfined compression of either 0% or 33% of the thickness of the specimen is applied prior to the sinusoidal translational shear test. The amplitude of the shear deformation is 25% of the length. The sinusoidal translational shear frequency is 1 Hz and 40 cycles which is chosen to emulate the stresses and heart rate induced naturally within aortic tissue. Aortic tissue, which is naturally load bearing, is loaded within the normal range of stresses of an aorta. The graphs' traits are compared with the same loads exerted on brain tissue, which is not naturally load bearing, to hypothesize what on the stress-strain graphs could correspond with damage. Brain tissue and aortic tissue should experience differently not only due to structural differences, but possibly due to damage as well. A specimen is tested at 2 Hz and 40 cycles to verify whether any phenomena found in the 1 Hz stress response are characteristic of other frequencies or if these phenomena only occur with a 1 Hz applied shear deformation.

## 3.4 Methods of Analysis

The shape and magnitude of the stress-strain data is compared for each compression and material.

### 3.4.1 Mullins Effect

Zuniga and Beatty (2002) propose that tensile stress softening in rubber can be modeled with an exponential function with three parameters (Equation 15). Taking a similar approach to their enriched form of the linear vibrations damping envelope equation, for the brain and artery tests the decreasing trend of the peaks on subsequent cycles is fit to a three parameter model. The equation for  $Y$ , the peak stress values with respect to time, is

$$Y = A \exp(-bt) + c. \quad (18)$$

The first term,  $A$ , controls the magnitude of the overall drop in the stress, the second term,  $b$ , influences the quickness of the drop, and the third term,  $c$ , allows the model to approximate the steady state value of the stress over time. A Matlab program is used to fit each curve and computes the equation variables (Section 7.1).

### 3.4.2 Signal Processing Analysis

One technique to determine the dominant frequencies within the stress versus time response is to subject the data to frequency filtering. Frequency filtering is a process that takes a current signal and applies a pass filter of a set range of frequencies. By expanding and restraining the band of frequencies allowed, the new signal shows whether the frequencies chosen are present in the original signal. A Matlab program is used to filter each stress curve (Section 7.1).

Fourier Series Decomposition is a method to represent a given periodic signal as a sum of multiple sine and cosine functions. In terms of  $\exp(2\pi i\omega t) = \cos(2\pi\omega t) + i \sin(2\pi\omega t)$ , the Fourier series equation is given by,

$$h(t) = \sum_{n=-\infty}^{n=\infty} a_n \exp(2\pi int). \quad (19)$$

The coefficient  $a_n$  is determined from orthogonality of the basis functions as

$$a_n = \frac{1}{T} \int_0^T h(t) e^{-2\pi i n t} dt \quad (20)$$

where  $T$  is the period.

The Fourier transform generalizes the expression to obtain the coefficients of the Fourier series

$$\begin{aligned} H(\omega) &= \int_{-\infty}^{\infty} h(t) e^{-i\omega t} dt \quad \text{or} \\ H(f) &= \int_{-\infty}^{\infty} h(t) e^{-i2\pi f t} dt \end{aligned} \quad (21)$$

where  $\omega$  is angular frequency and  $f$  is frequency given in Hz.

The signal can be described as a function in the time domain or the frequency domain. In the frequency domain, the function is complex which gives amplitude information as well as phase shift information at a given frequency. Using the Fourier transform, one can pass between the two domains. The inverse Fourier transform is (from the frequency to the time domain)

$$h(t) = \int_{-\infty}^{\infty} H(f) e^{2\pi i f t} df \quad (22)$$

where  $H(f)$  is the signal in the frequency domain and  $h(t)$  is the signal in the time domain.

One technique to compute the Fourier transform is Fast Fourier transform. Fast Fourier transform (FFT) is a technique to estimate the Fourier transform of a discrete periodic function. A magnitude spectrum graph displays the real and imaginary magnitudes of the function in the frequency domain and easily shows which frequencies in the signal are the most significant. A Matlab program is used to decompose each stress curve using fast Fourier transform (Section 7.1). A Fourier decomposition

analysis is applied to the displacement curve to verify that no artifacts exist.

The stress versus time and strain versus time data for each material is studied for the first three cycles to determine the lag-lead relationship between stress and strain for the initial response and how it changes with subsequent cycles. Since Fourier series can only accurately fit periodic functions, the Fourier series may not be able to fit the data; in that case Newland harmonic wavelet analysis is used. Harmonic wavelet analysis is different from the Fast Fourier Transform because instead of breaking the signal into harmonic sine functions that do not decay with time, the harmonic wavelet transform (HWT) breaks the signal into local wavelets that are defined over infinite time but have significant amplitudes in a finite time. Harmonic wavelets specifically involve orthogonal wavelets which creates easier mathematics and allows for a unique set of wavelets in a given signal (Newland 1994b). Harmonic wavelets take the form of

$$w(x) = \frac{\exp(i4\pi x) - \exp(i2\pi x)}{i2\pi x}. \quad (23)$$

Harmonic wavelet transform is used to capture dominant frequencies ( $j$ -level) and the times ( $k$ -level translation) that occur within the data. The harmonic wavelet written in terms of  $j$  and  $k$  is

$$w(2^j x - k) = \frac{\exp(i4\pi(2^j x - k)) - \exp(i2\pi(2^j x - k))}{i2\pi(2^j x - k)}. \quad (24)$$

The translations in the time domain within a frequency level is induced by  $k$  from the wavelet's Fourier transform in the frequency domain (Newland 1993). An increase in  $k$  level corresponds with a further shift in time. A wavelet with  $j = 1$ ,  $k = 0$  and that is purely real is shown in Figure 16.

The harmonic characteristic of the wavelets allow for the interpretation of the levels and translations are confined to an octave band of frequencies. The harmonic wavelet transform uses a FFT and inverse FFT process to analyze discrete experi-

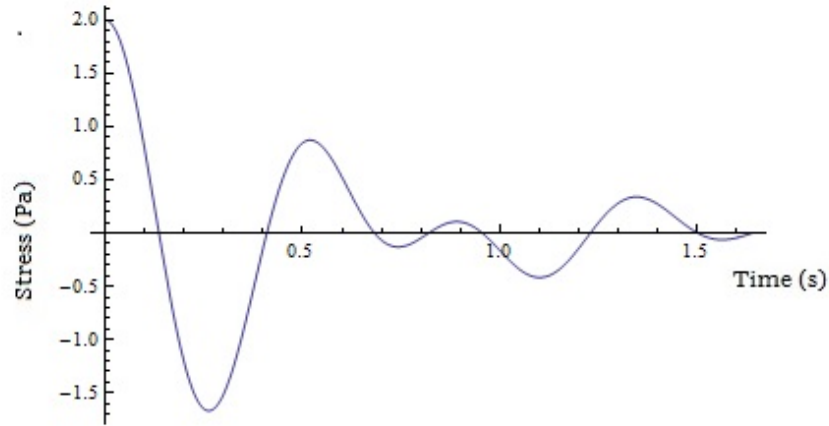


Figure 16: A real wavelet graphed versus time for  $j = 1$  and  $k = 0$ .

mental data, which does not need to be periodic or sinusoidal. This method looks at frequency levels that correspond to frequency ranges starting at  $j = 0$  and a frequency range from  $\frac{2\pi}{T}$  to  $\frac{4\pi}{T}$  where  $T$  is the total time of the data being evaluated. Each frequency range increases in width as the frequency level increases. The frequency range doubles with each sequential  $j$  level increase and the equation for the frequency range at any  $j$  level is

$$\frac{(2\pi)2^j}{T} \leq f < \frac{(2\pi)2^{j+1}}{T}. \quad (25)$$

The total time of the experiment must be rounded down to a new evaluated time,  $T = 2^n$  for the FFT computations with the highest integer value of  $n$  so that  $2^n$  is less than the original total time. Therefore, the analysis is applied to the number of cycles that occur in time  $T$ . The component frequencies that can be identified are limited and not exact (since they are given in ranges) however this method finds the most prominent frequency ranges and the time intervals in which they occur. This method is very dependent on the number of data points; the more data points over a given time frame, the more frequencies that can be analyzed and the more tightly defined time intervals can be examined at a given  $j$  level (Equation 25). A faster programmed sampling time gives more points in a test, but the sampling rate on



the Bose test machine does have a limit (0.0002 s). This method can give us the transient information as well as information on how the frequency components may change with time.

Both the FFT and the harmonic wavelet method give information about the average value of the curve or measure of symmetry around the time-axis, given as a zero frequency level amplitude. They also both provide information about the importance or dominance of certain frequencies.

To determine the goodness of fit of the decomposition as compared to the original curve, the  $L_2$  error is calculated as the ratio of the  $L_2$  norm of the difference between the curves to the  $L_2$  norm of the original curve

$$\frac{|G - g|}{|g|} = \frac{\sqrt{\sum |G - g|^2}}{\sqrt{\sum |g|^2}} \quad (26)$$

where  $G$  is the decomposed function and  $g$  is the original stress signal. A Matlab program is used to organize the wavelets into 20 bins in order of their magnitudes. The bins magnitude ranges are determined by a step size of  $\frac{max-min}{20}$  where the maximum and minimum wavelet magnitudes are calculated (Section 7.1). An increase in bin number corresponds to a decrease in wavelet amplitude. The bin number captures the highest magnitude wavelet in bin number 1 with decreasing magnitudes as the bin number increases.

### 3.4.3 Statistical Analysis

Two-factor ANOVA (Analysis of Variance) tests are used to examine statistical dependence of the stress response on compression and material. Parts of the stress versus time response are analyzed including the first stress peak magnitude, the magnitude of stress drop over the cycles ( $A$ ), the quickness of stress drop over the cycles ( $b$ ), and the steady state response ( $c$ ) (Equation 18). Two-factor ANOVA tests are

computed to determine the dependence of the Fourier series coefficients for 0 Hz, 1 Hz, and 3 Hz on material and compression.

Reproducibility, a relative standard deviation, is calculated for the numerical values used as

$$R = \frac{SD}{AVG} \quad (27)$$

where  $SD$  is the standard deviation and  $AVG$  is the average of a set of values. Reproducibility gives relative meaning to the standard deviation. For example, if the standard deviation is 10 and the average is 1000, the reproducibility is 0.01, but if the average is 5 the reproducibility is 2. A reproducibility factor of less than 1 shows a relatively small standard deviation and therefore a likely reproducible set of ANOVA statistics. Reproducibility loses its meaning as the average approaches zero.

## 4 Results

The cerebral arteries and brain lie in close proximity in the head so that during a trauma, the brain tissue and the arteries are likely affected at the same time. The bovine aorta is a model for the cerebral arteries since human cerebral arteries are not available for testing. Brain and aortic tissue were tested under sinusoidal translational shear and fixed unconfined compression. Particularly of interest is the difference between brain tissue, a naturally non-load bearing material, and aortic tissue, a naturally load bearing material in vivo. The results are presented in two sections, qualitative and quantitative. First, the qualitative section provides graphs for each type of test and analysis using values that can be pulled from the graphs: first peak stress amplitude, change in stress amplitude, symmetry of response, and the time shift between the stress response and the applied deformation response. Next, the quantitative section provides signal analysis of each type of test to determine the frequencies present in the stress response.

### 4.1 Qualitative Analysis

Throughout this study, repetitions of the same tests were performed not only to gather statistical evidence, but also because of the amount of specimen variability. Specimen variation in soft biological tissue stress responses exists based on animal to animal differences (e.g. size differences). With a lack of exact reproducibility, the tests were performed several times to gather information about the average and standard deviation of the data to better characterize and interpret the results.

From the 0% compression graphs (Figure 17, 19), it is clear that the mechanical behavior of the two tissues is not the same. Within this section, the magnitude of the stress amplitudes is compared for each tissue at both 0% compression and 33% compression. The first stress peak amplitude is specifically of interest because this

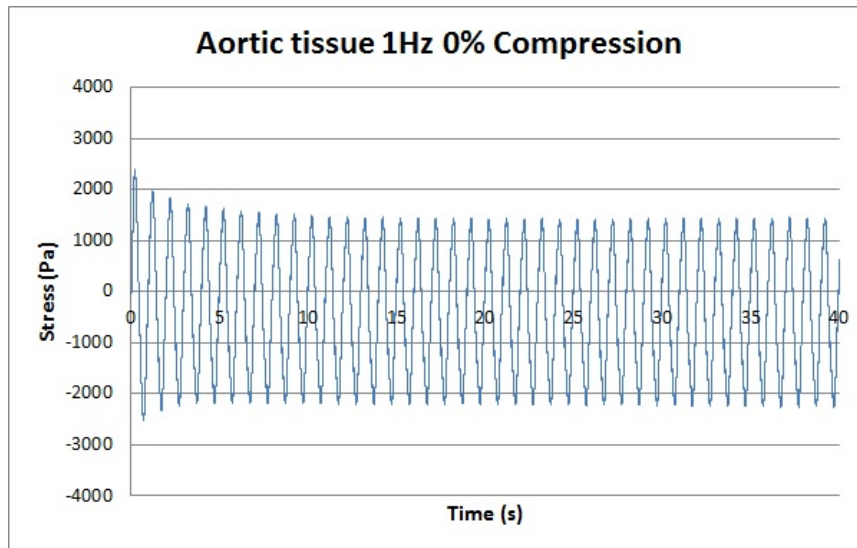


Figure 17: Stress versus time response of aortic tissue under 0% compression and 1 Hz, 25% translational shear strain (22515b).

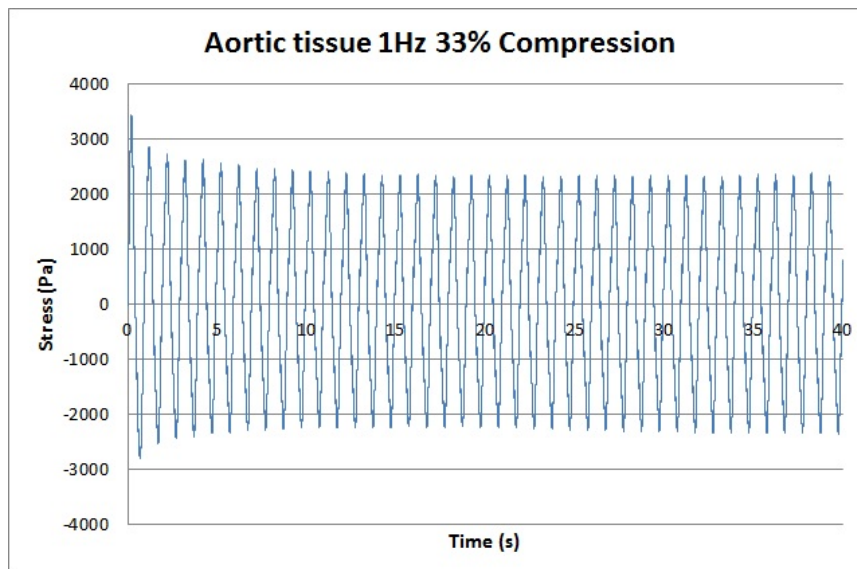


Figure 18: Stress versus time response of aortic tissue under 33% compression and 1 Hz, 25% translational shear strain (22515d).

is the tissues' initial mechanical response to deformation. The change in amplitude over time is of interest because this is the tissues' mechanical response to a repetitive deformation. The time shift between the stress versus time and strain versus time graphs is analyzed for the first 3 cycles and calculated as the time between each curve crossing through the horizontal axis. The shape of the stress graphs is checked for

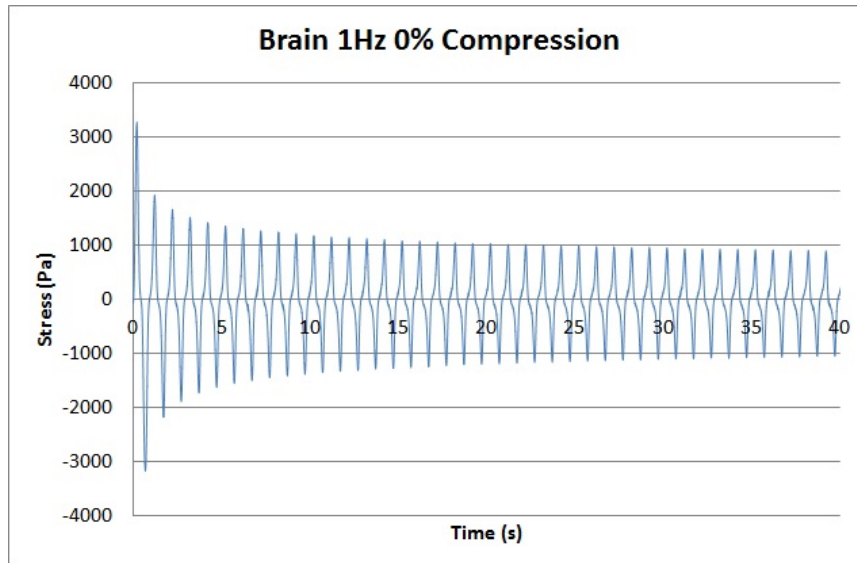


Figure 19: Stress versus time response of brain tissue under 0% compression and 1 Hz, 25% translational shear strain (20515a).

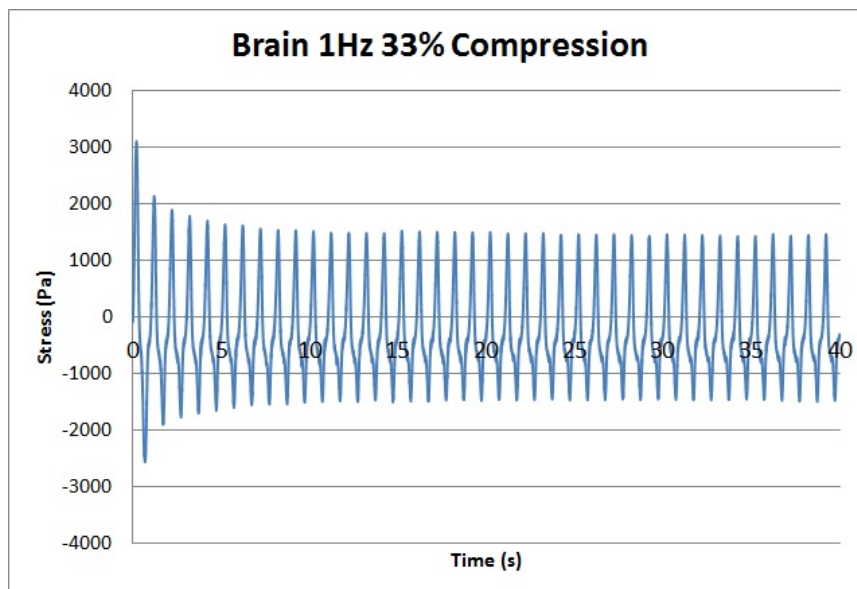


Figure 20: Stress versus time response of brain tissue under 33% compression and 1 Hz, 25% translational shear strain (12915a).

symmetry with respect to a vertical line through the center of a half cycle as well as with respect to the horizontal axis over all cycles. These graphical comparisons are meant to help understand the mechanical response of brain tissue as compared to a natural load carrying tissue.

#### 4.1.1 First Peak Amplitude of Sinusoidal Shear Response

The shear stress magnitude is largest on the first deformation cycle (Figure 17, 18, 19, 20). The brain and aortic tissue shear peak stress magnitudes under a deformation strain of 25% are nearly the same on the first deformation cycles and have average amplitudes of 2856 Pa and 2578 Pa respectively. It should be noted that the first peak stress magnitude response does vary by specimen.

Table 1 reports the peak shear stress which occurs on the first deformation cycle for 24 total specimens (6 of each type of test) of which 12 are under no compression and 12 are under 33% compression. A two-factor ANOVA with replication determines the statistical difference between the first peak stress of brain tissue and aortic tissue as well as the dependence on compression. The brain and aortic tissues do not show a statistically significant difference in the first stress peak magnitude ( $P=0.2723$ ). For both tissues, compression causes a significant increase in stress magnitude ( $P=0.014$ ). The standard deviation has little meaning when viewed alone. The reproducibility ratios for the peak stress magnitudes are less than 1 so these tests satisfy the criterion for repeatability used in biomechanics.

#### 4.1.2 Mullins Effect in Shear Stress Response to Translational Shear Deformation

The Mullins effect (Section 3.4.1) under sinusoidal deformation describes stress softening in which the stress magnitude of subsequent reloading cycles significantly decreases from the stress of the initial loading cycle. Most of the Mullins effect reports are for tensile deformation; however, in the present reported data for brain and aortic tissue a similar effect is seen in translational shear.

The stress response of both materials displays a transient part of about 6-10 cycles during which the peak stress amplitudes decrease over time (Figure 17, 18, 19,

Table 1: Brain and Aortic Tissue 40 Cycles at 0% and 33% Compression

	Test Name	First Peak Stress (Pa)	A	b	c
Aorta, 0%	22515b	2275.38	972.2	0.3715	1440.4
	22515c	3338.13	1011.8	0.1734	1995.2
	40915a	1640.45	147.7	0.1286	1588.9
	40915b	1752.18	208.4	0.153	1642.8
	40915c	2100.98	270.1	0.1465	1945.6
	40915d	2430.7	213.5	0.1093	2325.2
	AVG		2256.303	470.6167	0.180383
SD		609.6996	405.9098	0.096132	325.7441
R		0.2702	0.8625	0.5329	0.1786
Aorta, 33%	22515d	2294.4	1063.2	0.4276	2372.6
	22515e	2741.3	587.1	0.7343	3344.5
	22515f	2043.7	405.5	0.5862	1661.9
	40915e	3719.6	496.6	0.1335	3273.4
	40915f	3259.3	863.1	0.1612	5542.2
	40915g	3346.3	853.4	0.5633	2833.9
	AVG		2900.8	711.48	0.43435
SD		651.9	253.8	0.2428	1318.4
R		0.2247	0.3567	0.5590	0.4157
Brain, 0%	20515a	2695.0	1822.2	0.7917	1095.7
	20515b	2485.2	1666.4	0.5695	904.2
	21915a	3284.9	2376	0.2705	810.7
	21915b	2252.2	1233.8	0.0758	572.7
	42315b	3302.7	2250.5	0.6012	1196.6
	42315c	2714.1	1997.3	0.7096	933.07
	AVG		2789.0	1891.0	0.5030
SD		425.38	415.41	0.2744	219.2
R		0.1525	0.2196	0.5456	0.2385
Brain, 33%	12915a	3116.0	1794.1	0.6526	1491
	42315d	2839.4	2063.1	0.6929	951.6
	42315e	4696.5	4732.8	1.1969	1001.7
	42315f	4058.8	2828.6	0.6562	1446.6
	42315g	4805.5	4235.4	1.0737	1388
	42315h	3001.5	2556.7	0.6678	656.0
	AVG		3753.0	3035.1	0.8233
SD		882.7	1189.8	0.2451	336.4
R		0.2352	0.3920	0.2977	0.2910

20). Table 1 lists the parameter values  $A$ ,  $b$ , and  $c$  for the 24 specimens found from Equation 18. Brain tissue experiences a much larger drop in peak stress magnitude in the first few cycles than aortic tissue, while aortic tissue has a more gradual decay in peak stress magnitude.

For both tissues, after the stress drop over the first few cycles, the stress peaks appear to level out with a more gradual change in stress. However, in some cases for aortic tissue, the stress peak amplitude gradually decreases as the number of cycles increases and in other cases there is a slight stiffening past about 20 cycles, or increase in stress peak amplitude. The brain tissue stress response does not exhibit any stiffening, only a stress drop in the initial deformation cycles.

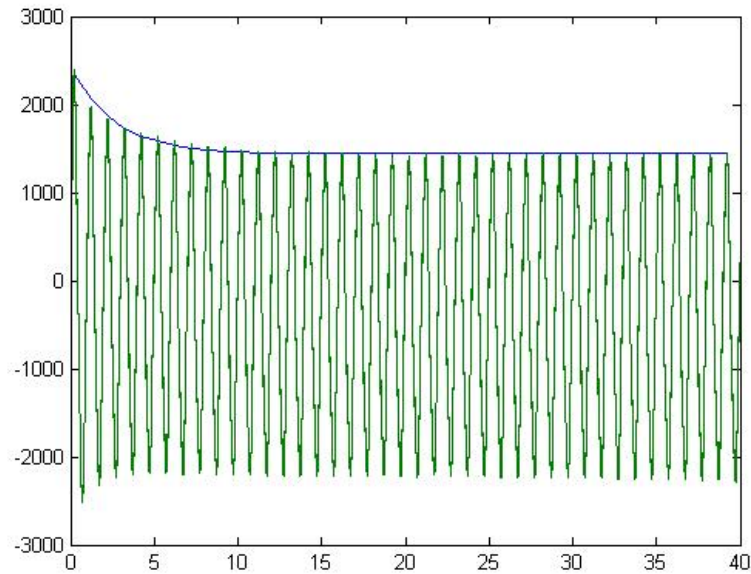


Figure 21: Stress versus time response and exponential fit curve of aortic tissue under 0% compression and 1 Hz, 25% translational shear strain.

The exponential fit is not exact (Figure 21, 22, 23, 24), but the fit does provide insight on whether the stress response is similar to Mullins effect. A two-factor ANOVA with replication is used to evaluate the effect of tissue and compression on each coefficient in the decay equation. The first term,  $A$ , from the exponential fit for brain tissue is significantly larger than that for the aortic tissue ( $P=1.3E-$



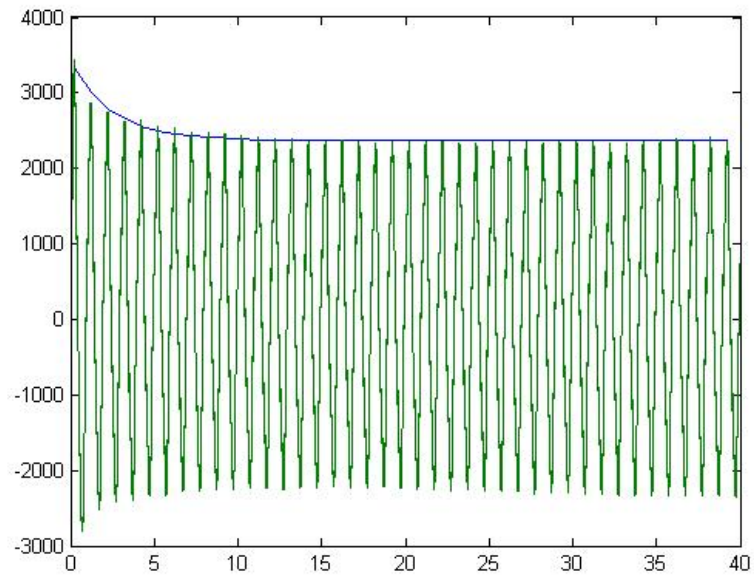


Figure 22: Stress versus time response and exponential fit curve of aortic tissue under 33% compression and 1 Hz, 25% translational shear strain.

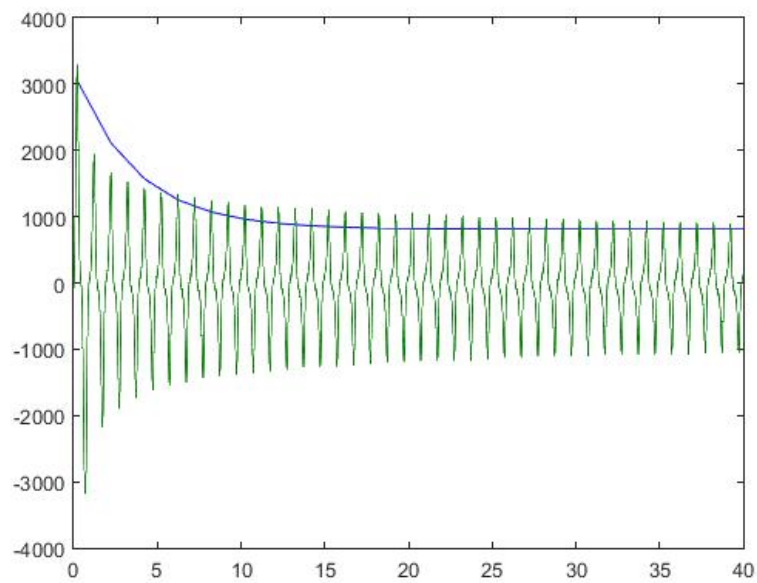


Figure 23: Stress versus time response and exponential fit curve of brain tissue under 0% compression and 1 Hz, 25% translational shear strain.

06). The compression causes a significant increase in the first exponential fit term for both tissues ( $P=0.020$ ). The second term,  $b$ , for the fit, which corresponds to

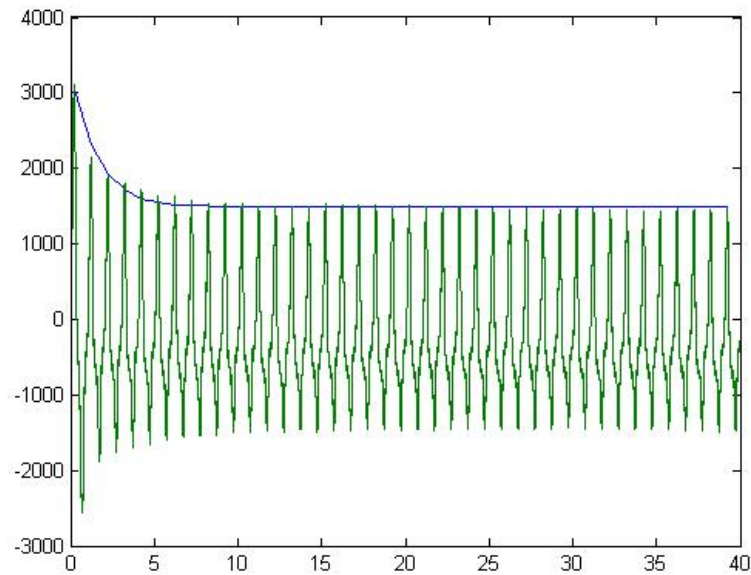


Figure 24: Stress versus time response and exponential fit curve of brain tissue under 33% compression and 1 Hz, 25% translational shear strain.

the quickness of the drop in stress is also larger (Table 1) for brain tissue than for aortic tissue ( $P=0.005$ ). Compression causes an increase in the second term,  $b$ , for both tissues ( $P=0.0009$ ). The third term,  $c$ , corresponds to the steady state stress magnitude which is higher for the compressed tests for both specimens as compared to each materials uncompressed test ( $P=6.13E-05$ ). The third term is lower for brain tissue than aortic tissue ( $P=0.0125$ ). The reproducibility factors for  $A$ ,  $b$ , and  $c$  are all less than 1.

### 4.1.3 Symmetry of one Load-Unload Cycle

About the vertical axis through the peak of a half cycle, the aortic tissue is nearly symmetric and the brain tissue is not symmetric. The load response of brain tissue displays ‘shoulders’, an asymmetric deformity causing opposing concavity on each cycle (adding more inflection points on the curve) that differs from a pure sine wave signal (Figure 25). The shoulders break symmetry about the vertical line through the peak because they are at different locations on the loading side of a half cycle as compared to the unloading side. No visible shoulder appears on the first deformation of the brain (Figure 19, 20). The aortic tissue stress response in a single half cycle is nearly symmetric with respect to the vertical axis that crosses through the peak values. No shoulders are visibly present in the aortic tissue response (Figure 17, 18); this difference indicates that some component of one of the tissues significantly influences its stress response.

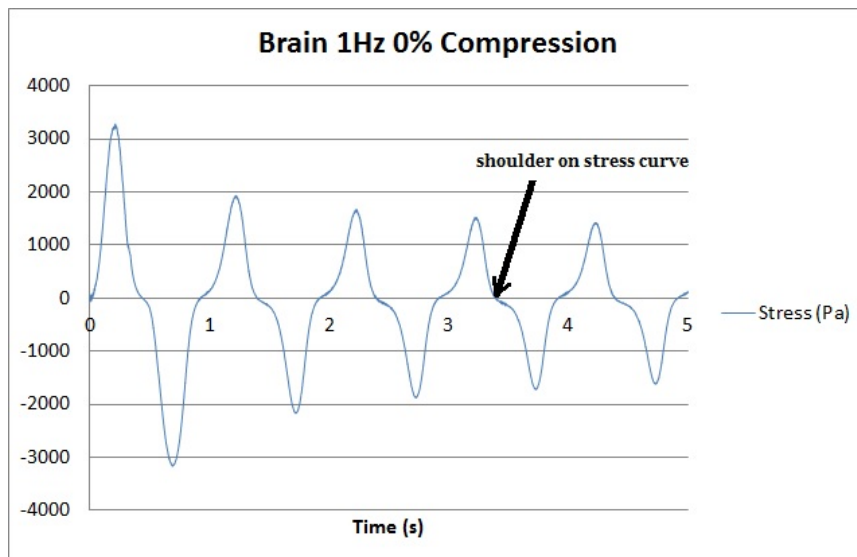


Figure 25: Shoulder shown on a stress versus time curve for brain tissue under 0% compression and 1 Hz, 25% translational shear strain.

#### 4.1.4 Symmetry about the Horizontal Axis

The vertical symmetry with respect to the horizontal axis in a single cycle varies with specimen and is not always symmetric because the maximum positive and negative stresses are unequal in magnitude. The symmetry with respect to the time axis can be seen more clearly toward the last set of cycles when the stress peaks are mostly constant (Figure 17, 18, 19, 20). For the compression tests for both specimens, the symmetry about the horizontal axis is more offset (when the average magnitude of the entire stress signal is nonzero) than the non-compressed tests so it is not symmetrical about the horizontal time axis. The stress response of the compressed tissue tests shows a shift about the horizontal axis (sometimes in the positive and sometimes negative direction) causing a difference in the positive and negative stress magnitudes. For the compressed brain tissue tests, the ‘shoulders’ shift with respect to the horizontal axis and no longer occur on the horizontal axis, but rather on the negative side of the stress response (Figure 20).

#### 4.1.5 Time Shift

A time shift on each cycle is defined as the time between the stress versus time graph and the strain versus time graph as they cross through the horizontal time axis on the corresponding cycle (Section 2.1). The time shift that is defined here is more general than the phase shift that is commonly known for sine curves because the phase shift involving sine curves is constant over many cycles. Aortic tissue stress versus time response with respect to the strain versus time data has a time shift that is smaller in magnitude than the time shift in brain tissue. The aortic tissue stress time shift creates a lag in the stress (the stress curve crosses the horizontal time axis after the deformation reaches zero) for most tests while some have small amplitude time shifts (near zero). Conversely, the brain tissue stress time shift creates lead in the stress (the stress curve crosses the horizontal axis before the deformation reaches zero).

For aortic tissue, the average time shift is approximately 0.04 s with displacement leading the stress curve (Figure 26). For brain tissue, the average time shift is approximately 0.1 s with the stress leading the displacement curve. The brain tissue stress versus time response is quasiperiodic; the shift changes over time within the brain stress data and typically increases and eventually stabilizes (Figure 27, 28) (Table 2). All reproducibility factors are less than 1 from Table 2.

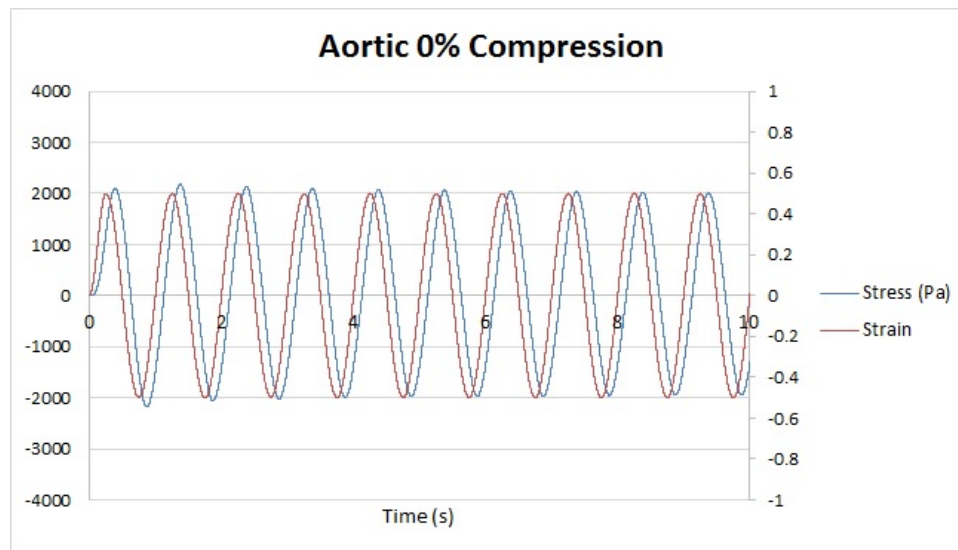


Figure 26: Strain leads stress for the aortic tissue stress versus time response under 0% compression and 1 Hz, 25% translational shear strain.

Table 2: Brain Tissue Time Shift at the End of Each of the First 3 Deformation Cycles

	Test Name	Shift 1	Shift 2	Shift3
Brain, 0%				
	20515a	0.0914	0.1004	0.1029
	20515b	0.0776	0.0938	0.0956
	21915a	0.0674	0.1053	0.109
	21915b	0.0626	0.063	0.0638
	42315b	0.0742	0.096	0.1119
	42315c	0.0864	0.077	0.1182
AVG		0.0766	0.0892	0.1002
SD		0.0109	0.0160	0.0194
R		0.1433	0.1797	0.1940
Brain, 33%				
	12915a	0.1376	0.1524	0.1529
	42315d	0.1012	0.112	0.114
	42315e	0.0835	0.1282	0.1348
	42315f	0.0879	0.0943	0.1009
	42315g	0.1064	0.1156	0.1187
	42315h	0.0883	0.1022	0.108
AVG		0.1008	0.1174	0.1215
SD		0.02003	0.02068	0.01914
R		0.1987	0.1760	0.1575

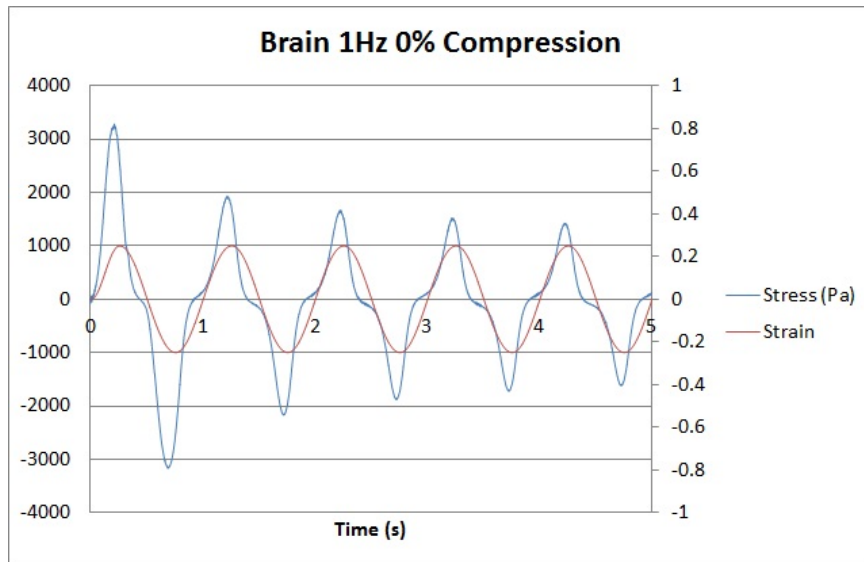


Figure 27: Stress leads strain for the brain tissue stress versus time response under 0% compression and 1 Hz, 25% translational shear strain.

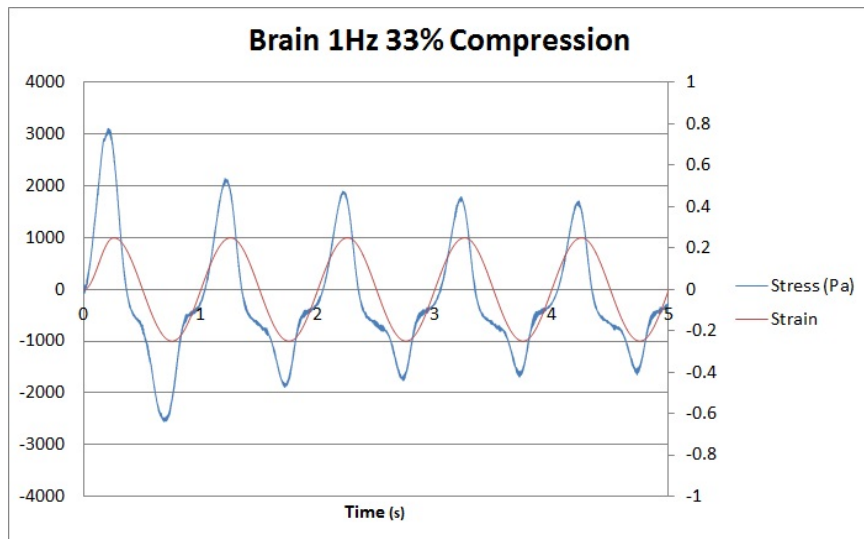


Figure 28: Stress leads strain for the brain tissue stress versus time response under 33% compression and 1 Hz, 25% translational shear strain. The time shift changes on subsequent cycles and is different for the front and back side of a half cycle.

#### 4.1.6 Limit Cycle

Stress versus strain graphs over 40 cycles help to visualize whether a limit cycle exists and the presence of hysteresis (Figure 29, 30, 31, 32). The stress versus strain graphs are compared to the stress versus time analysis of the Mullins effect to help visualize the transient response. The number of cycles prior to the limit cycle is related to the quickness of stress drop variable,  $b$ , from the exponential fit equation (18); the higher the  $b$  value in the exponential fit equation, the quicker the stress drops and the fewer number of cycles before steady state. The magnitude of the drop in the stress-strain curves over the first few cycles is related to the magnitude of stress drop variable,  $A$ , from the exponential fit equation.

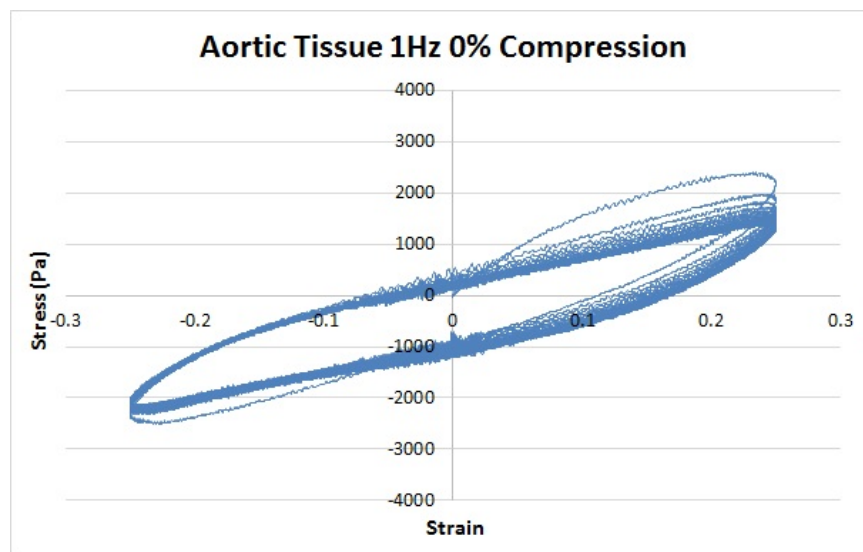


Figure 29: Stress versus strain curve for aortic tissue under 0% compression and 1 Hz, 25% translational shear strain.

The aortic tissue stress-strain graphs are a much different shape than the brain tissue stress-strain graphs; the brain tissue cycles have more of a pronounced ‘S’ shape and are much thinner in the sense that the area within the loop is smaller than that of the aortic tissue stress-strain cycles (Figure 29, 30, 31, 32). The stress-strain graphs for brain tissue exhibit a flat section at low strains and then harden; this flattening/hardening does not occur in the aortic tissue and does not exist on



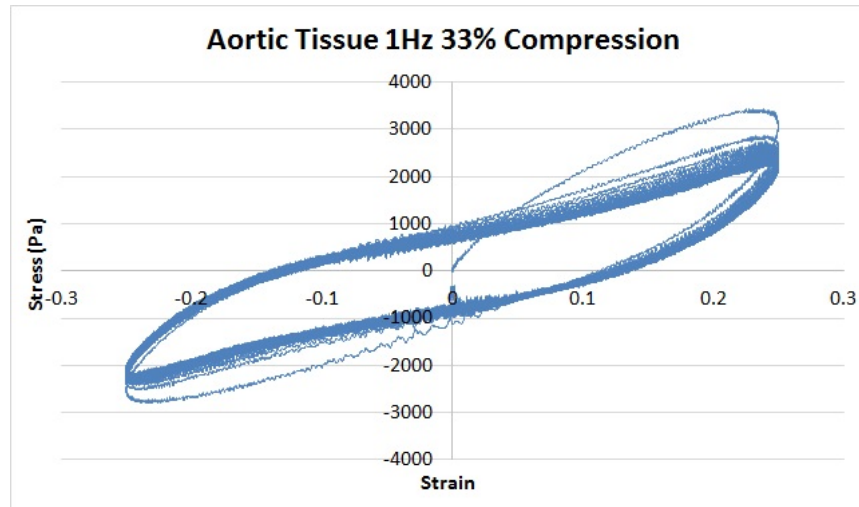


Figure 30: Stress versus strain curve for aortic tissue under 33% compression and 1 Hz, 25% translational shear strain.

the first cycle of the brain tissue response. The flat region of the brain tissue stress-strain response correlates to the shoulder in the brain tissue stress-time response. Compression causes an increase in the area within the stress-strain cycles for both materials. If the material were elastic, then there would be no area within the cycles. The area in the loops of the stress-strain curves are often used to measure to amount of energy absorbed and dissipated, however no attempt was made to measure the area enclosed because it is not clear that in this case the area enclosed is the energy lost; many other factors may cause the appearance of energy dissipation (eg. fluid redistribution and solid phase damage). The compression in brain tissue causes a negative shift of the center of the loop (Figure 32) which correlates to the shift in the stress from the stress-time graph (Figure 20). The loops are graphed clockwise through time so the gap between the horizontal axis and where the stress-strain curve crosses through the zero-strain axis verifies that stress leads strain for the brain tissue because stress is zero before strain is zero.

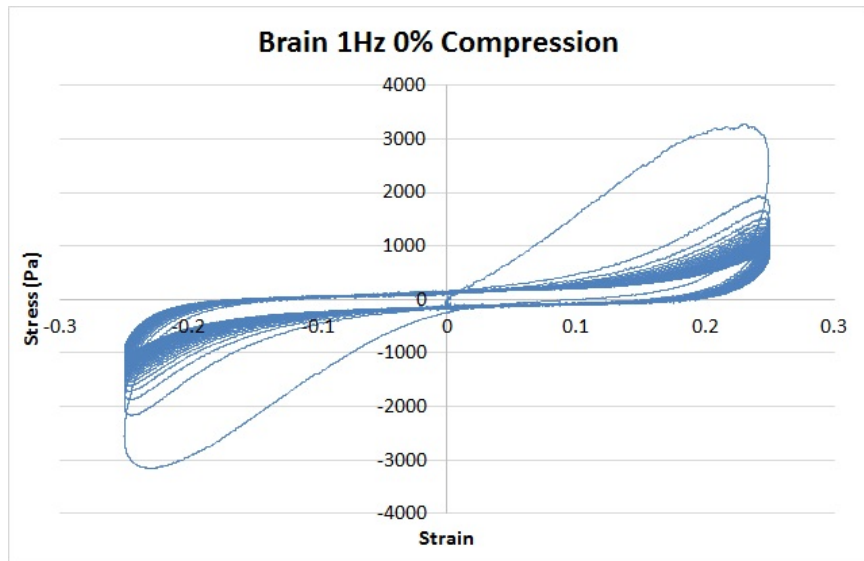


Figure 31: Stress versus strain curve for brain tissue under 0% compression and 1 Hz, 25% translational shear strain.

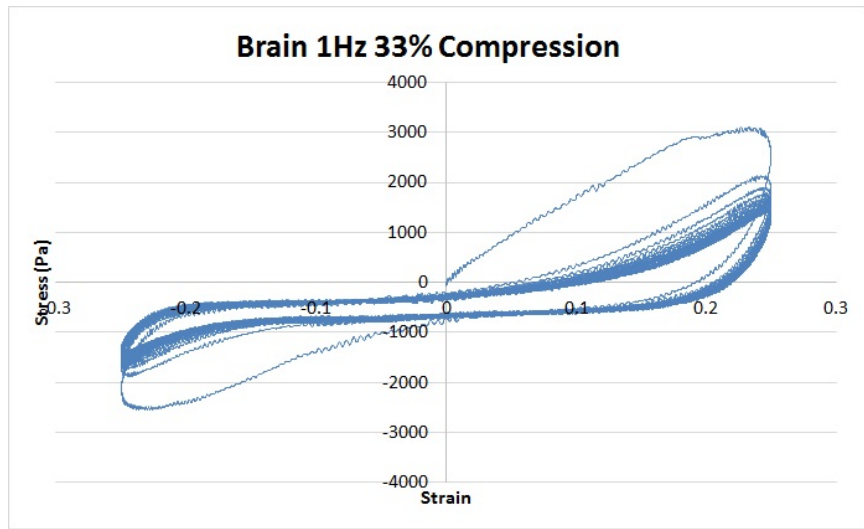


Figure 32: Stress versus strain curve for brain tissue under 33% compression and 1 Hz, 25% translational shear strain.

## 4.2 Frequency Decomposition of the Stress Response

One long-term goal is to correlate the frequency components of the stress response to the behavior of the fluid and solid portions of the tissues that might cause differences in the response such as the shoulders in the brain tissue. A frequency filter is used to determine the main frequencies responsible for the shoulders in the brain tissue stress response. The frequency of the stress response and the magnitude of each frequency component from each tissue are further examined in a Fourier series decomposition, and in a harmonic wavelet decomposition as described in the Methods section (3.4.2).

### 4.2.1 Frequency Filter

Matlab is used to apply a pass filter on the uncompressed brain stress response data to graph only the part of the stress versus time signal with a frequency response within the frequency range given. Expanding and constricting the pass filter from 0-1 Hz, 2-3 Hz and 0-3 Hz, shows the shear stress response of brain tissue to an applied 1 Hz sinusoidal deformation has a 1 Hz component which is the same as the applied strain frequency and a 3 Hz component which captures the shoulders in the stress response (Figure 33). The fit is not perfect with only the sum of 1 and 3 Hz components, however the sum captures the majority of the response (Figure 34). Other higher frequencies may also exist to capture the rest of the signal response.

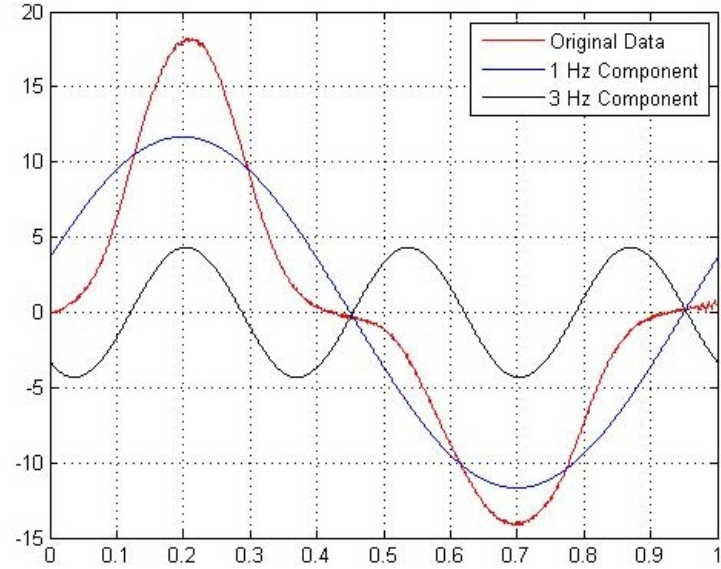


Figure 33: Frequency decomposition using two pass filters for 1 Hz and 3 Hz, of a original stress versus time curve for brain tissue under 0% compression and 1 Hz, 25% translational shear strain.

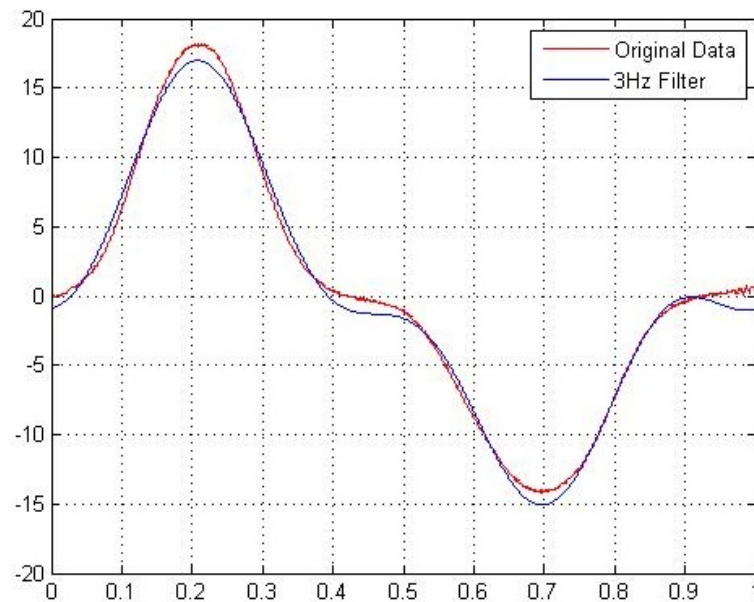


Figure 34: Sum of 1 Hz and 3 Hz curves detected from pass filters and original stress versus time curve for brain tissue under 0% compression and 1 Hz, 25% translational shear strain.

### 4.2.2 Fourier Series Analysis

To verify the shape and frequency of the mover displacement amplitude and to ensure that no artifacts in the controlled displacement can account for some characteristics of the shear stress response, Fourier series decomposition is used to analyze the displacement versus time data.

The frequencies extracted from the BOSE displacement versus time data for a programmed displacement amplitude of 3 mm at 1 Hz are 0, 1, and 3 Hz with Fourier coefficient amplitudes respectively 0.1547, 2.9916, and 0.0129 (Figure 35, 36). The most significant frequency is 1 Hz with small amplitude frequencies of 0 and 3 Hz so the applied displacement is close to a 1 Hz signal. Figure 35 is a frequency spectrum graph which displays the magnitude,  $Y(t)$  (in mm), of each sine function with respect to each frequency. Figure 36 is the Fourier decomposition displacement versus time curve plotted on top of the original displacement data.

The Bose displacement mover is electromagnetically controlled which allows the mover to move nearly friction-free as compared to hydraulic testing machines. Further sometimes during testing with hydraulic machines, spurious waves are induced in the hydraulic fluid that can add components to the controlled displacement of other hydraulic testing machines.

The frequency components of the shear stress response for each material at 0% and 33% compression are analyzed by a Fourier series decomposition. In particular, Fourier series decomposition is used to further examine the 3 Hz frequency component for the brain tissue response determined from the frequency pass filter analysis. For both aortic tissue and brain tissue, the significant frequencies from the Fourier series decomposition are 0, 1, and 3 Hz (Figure 37, 39). The reproducibility factor was less than 1 for all of the 1 Hz and 3 Hz components which are most significant due to their large magnitudes (Table 3). Small 2 Hz and 4 Hz components appear in some tests. A two-factor ANOVA with replication is used to determine the significance of tissue

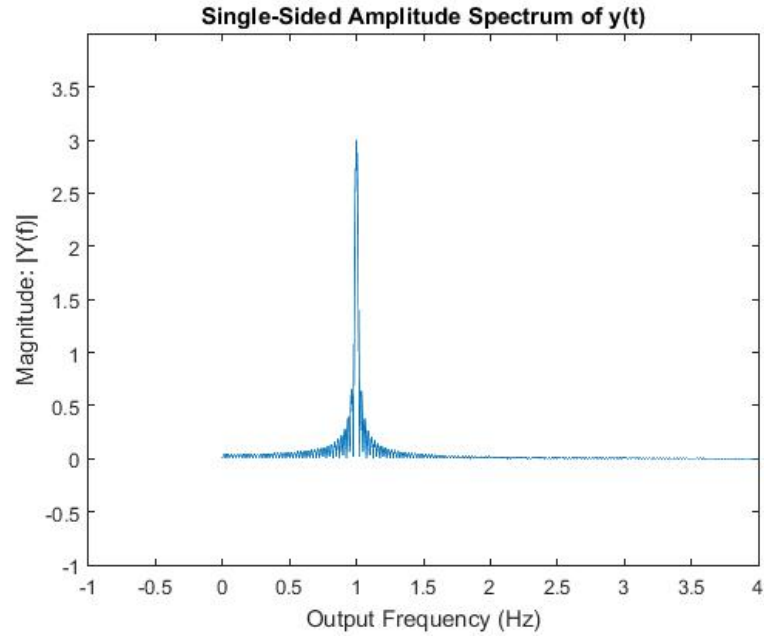


Figure 35: Fourier coefficient magnitudes versus frequency for BOSE displacement mover at 1 Hz and 3 mm amplitude.

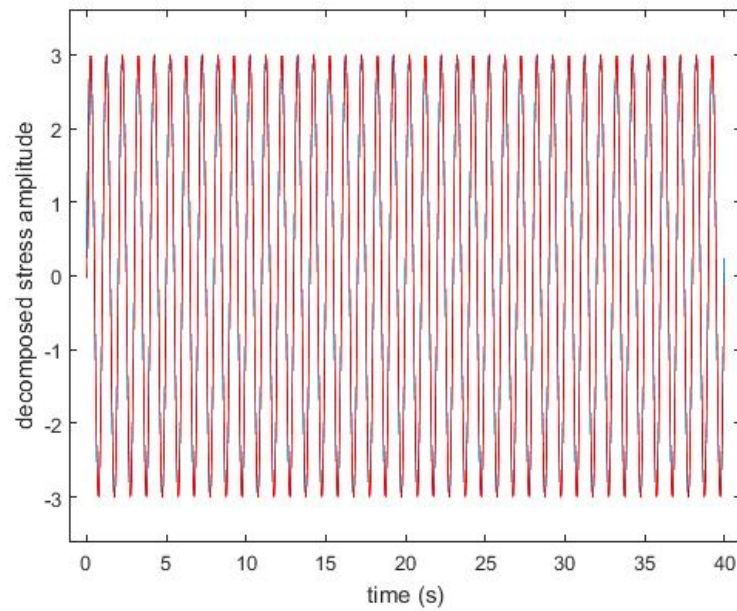


Figure 36: Fourier series decomposition curve (blue) and original curve (red) for BOSE displacement mover at 1 Hz and 3 mm amplitude. The two curves lie on top of each other.

and compression on the Fourier coefficients for each dominant frequency (0, 1, and 3 Hz). The magnitude of the Fourier coefficient for the 0 Hz component corresponds

to a magnitude shift or the average stress value and did not significantly depend on tissue type or compression. The 0 Hz Fourier coefficient is not statistically different with respect to tissue type or compression. The 1 Hz Fourier coefficient is higher in aortic tissue ( $P=1.2E-05$ ) and under 33% compression is higher than 0% compression in both materials ( $P=0.051$ ). The 3 Hz Fourier coefficient is higher in brain tissue ( $P=8.87E-07$ ) and is not statistically affected by compression, however visually the shoulders are influenced by compression as a shift toward the negative stress side with respect to the horizontal axis (Figure 20).

The Fourier Series Decomposition cannot model the transient portion of either set of data (Figure 38, 40). The brain has a quasiperiodic stress response (Table 2) that makes the Fourier series not able to model it correctly since the Fourier series summands are periodic sine functions each of which has a fixed phase shift.

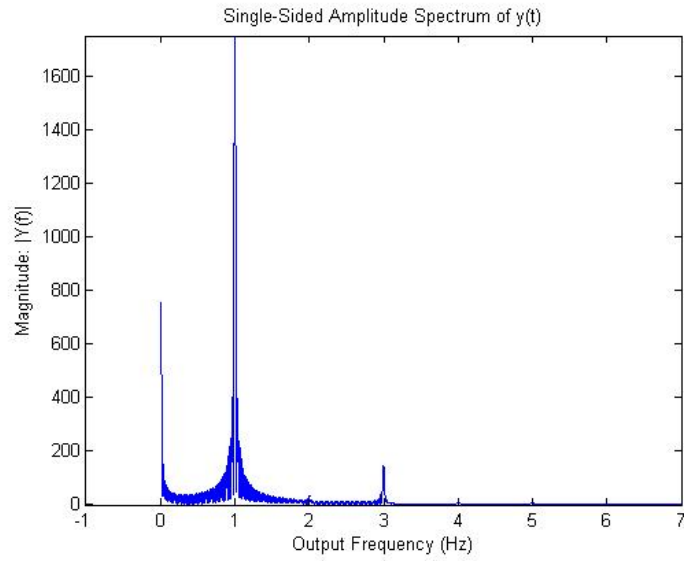


Figure 37: Fourier coefficient magnitudes versus frequency for aortic tissue under 1 Hz, 0% compression, 25% translational shear strain (22515b).

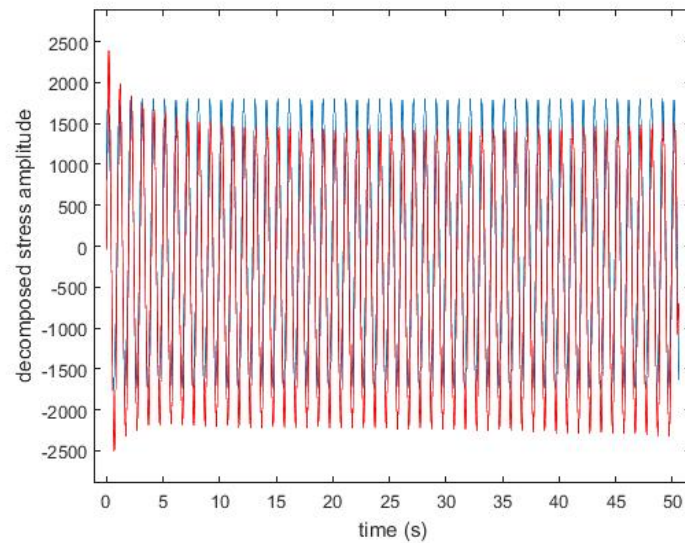


Figure 38: Fourier decomposition curve versus time (blue) and original stress versus time (red) curve for aortic tissue under 1 Hz, 25% translational strain (22515b).



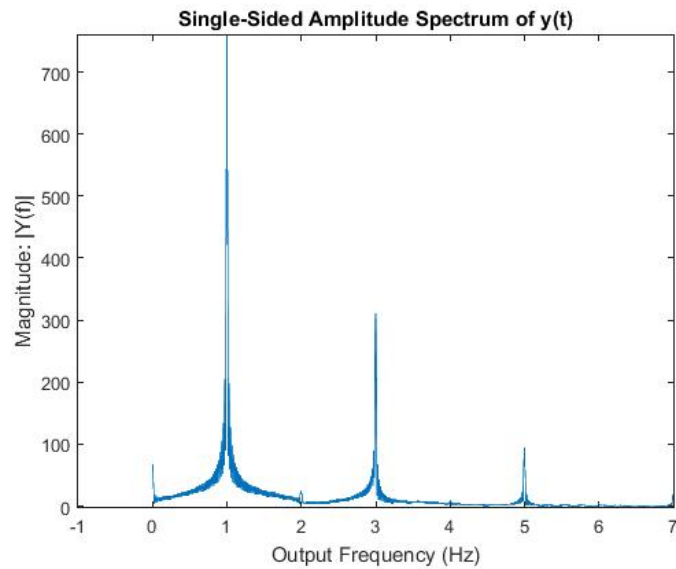


Figure 39: Fourier coefficient magnitudes versus frequency for brain tissue under 1 Hz, 0% compression, 25% translational shear strain (21915a).

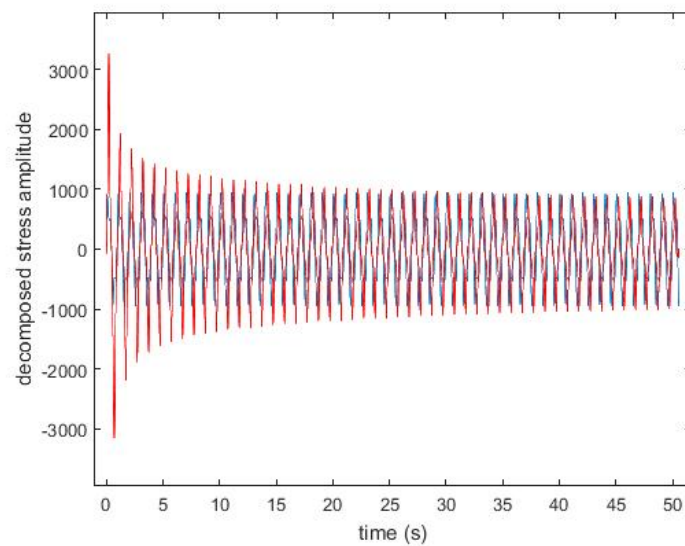


Figure 40: Fourier decomposition curve versus time (blue) and original stress versus time (red) curve for brain tissue under 1 Hz, 25% translational strain (21915a).

Table 3: Fourier Coefficients for Frequencies 0-6 Hz of Shear Stress Response (Pa)

	0 Hz	1 Hz	2 Hz	3 Hz	4 Hz	5 Hz	6 Hz
Artery, 0%							
22515b	755.8	1749.5	32.4	144.4	15.1	11.8	2.2
22515c	1092	2613.6	46.4	187.4	33.4	12.5	3.9
40915a	86.8	1621.3	0	18.6	0.7	0.9	0.3
40915b	89.8	1639.8	0	32.8	0.9	1.1	0
40915c	102.6	1885.3	21.4	39.9	0.8	0.5	0
40915d	121.7	2274.7	31.4	32.9	0	0	0
AVG	374.7833	1964.0333	21.9333	76	8.4833	4.4666	1.0666
SD	438.6019	398.3133	18.7628	71.2886	13.5181	5.9674	1.6317
R	1.1702	0.2028	0.8554	0.9380	1.5935	1.3360	1.5297
Artery, 33%							
22515d	121.5	2110.5	52.7	278.9	14.7	16.5	4
22515e	138.2	2969.4	132.6	175	13.4	18.2	0
22515f	76.5	1638.6	51	75.5	9.5	11.5	2.6
40915e	178.2	3229.8	0	41.2	0	1.4	0
40915f	299.1	5561.9	88.6	80.7	3.1	2.4	0
40915g	257.3	2600.4	25	68.7	2.2	1.3	0
AVG	178.4666	3018.4333	58.3166	120	7.15	8.55	1.1
SD	84.8893	1372.5405	46.9702	90.1555	6.2227	7.8298	1.7606
R	0.4756	0.4547	0.8054	0.7512	0.8703	0.9157	1.6006
Brain, 0%							
20515a	59.8	717.4	0	324	0	92	5.1
20515b	53.4	629.6	0	265.5	0	68.2	2.6
21915a	67.8	757.8	25	310.8	0	93.2	4.2
21915b	68.1	690.9	25	280.1	16.7	73.1	4.5
42315b	66.8	810.1	49.7	352.5	16.4	104.8	3.4
42315c	56.6	642.2	41	282.4	19.2	84.9	4.8
AVG	62.0833	708	23.45	302.55	8.7166	84.6	4.1
SD	6.35308	68.9368	20.5020	32.5757	9.5980	14.6977	0.9380
R	0.1023	0.0973	0.8742	0.1076	1.101	0.1737	0.2288
Brain, 33%							
12915a	523.6	1041.5	270	388.9	32.2	106.2	13.9
42315d	58.9	713.5	41.3	265.2	9.7	78.2	0
42315e	132.1	811.1	0	320.7	0	98.3	0
42315f	86.5	1092.8	33.8	391.5	0	101.8	0
42315g	115	966.6	75.1	350	17.7	103.5	0
42315h	56.8	625.7	0	166	0	48.7	2.1
AVG	162.15	875.2	70.0333	313.7166	9.9333	89.45	2.6666
SD	179.5852	187.5448	101.9412	86.3042	13.0552	22.3424	5.5669
R	1.1075	0.2142	1.4556	0.2751	1.3142	0.2497	2.0875

### 4.2.3 Harmonic Wavelet Analysis

Fourier series decomposition provides information about the dominant frequencies present in the stress versus time response, but does not fit the data with precision since the shear stress response for brain tissue is not periodic. Harmonic wavelet analysis provides information about the change in amplitude and the location of the frequency components with respect to time. Figure 41 displays the same 0% compression brain test from Figure 40; it can be seen that the harmonic wavelet decomposition analysis has a better fit than the Fourier series decomposition analysis.

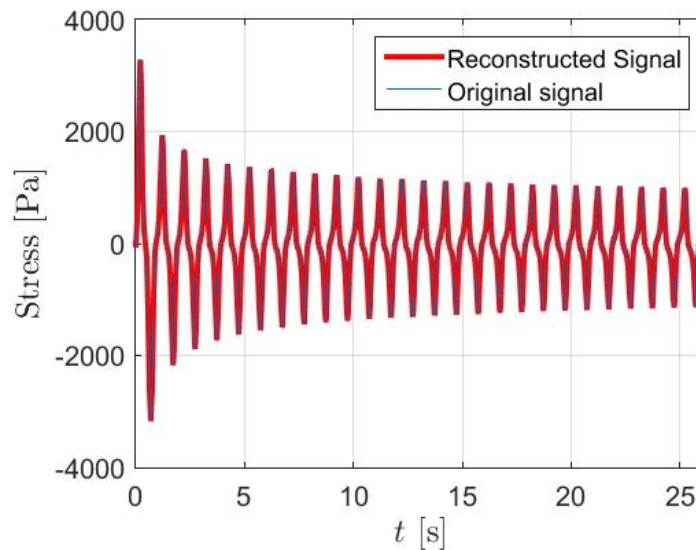


Figure 41: Harmonic wavelet decomposition curve and the original stress curve for brain tissue under 0% compression and 1 Hz, 25% translational shear strain. The curves lie on top of one another. (20515a)

Recall from Section 3.4.2, the harmonic wavelet analysis with a time step of 0.0002 s between sample points over 40 cycles requires a total evaluated time of  $T = 26.2142$ . The harmonic wavelet decomposition level  $j = 4$  corresponds to the frequency range of 0.6 – 1.2 Hz (Equation 25, Table 4) which is interpreted as the 1 Hz frequency response because the Fourier series decomposition contained dominant 1Hz and 3 Hz components. A  $j = 6$  level is interpreted as the 3 Hz frequency response by the same argument.

Table 4: Frequency Ranges for  $j$  Levels

$j$ level	Frequency Lower Bound (Hz)	Frequency Upper Bound (Hz)
1	0.1	0.2
2	0.2	0.3
3	0.3	0.6
4	0.6	1.2
5	1.2	2.4
6	2.4	4.9
7	4.9	9.8
8	9.8	19.5
9	19.5	39.1
10	39.1	78.1

The coefficient magnitude for the  $j = -1$  level corresponds to a vertical shift in the signal at all points (much like the Fourier series coefficient for the 0 Hz component). Table 5, 6, 7, and 8 show the  $j$  and  $k$  levels for the most significant wavelets computed from the harmonic wavelet decomposition. Figures 42, 43, 44, 45 show the harmonic wavelet decomposition of the dominant wavelets (only the wavelets in Tables 5 to 8) along with the original stress data.

The dominant frequency consistently present within the harmonic wavelet analysis for brain tissue and aortic tissue is 1 Hz, which is the applied deformation frequency. The brain tissue analysis detects a dominant 3 Hz component throughout the signal. The 3 Hz component does not appear at every value of  $k$ , however more 3 Hz components may exist within the many more small magnitude wavelets in Bin 20. Wavelets also interact and may overlap to create a 3 Hz signal in the areas in time where the  $k$  values are not dominant. The lowest  $k$  values (wavelets at the beginning of the signal in time) have the largest magnitude of all of the wavelets in the signal. The 3 Hz component only exists at low values of  $k$ , or in the first few cycles for the aortic tissue.

Table 5: Brain Tissue 40 Cycles at 0% Compression (20515a)

Bin number	$j$ level	$k$ level
1	4, 4	0, 1
7	4	2
11	4	4
12	4, 4	3, 5
13	4, 4, 4, 6	7, 8, 14, 1
14	4, 4, 4, 4	6, 10, 11, 13
15	4, 4, 5, 6	9, 12, 0, 2
16	6	0
17	4, 6, 6, 6	15, 3, 4, 7
18	6, 6, 6, 6, 6, 6, 6, 6, 6	5, 6, 9, 10, 11, 12, 14, 16, 19

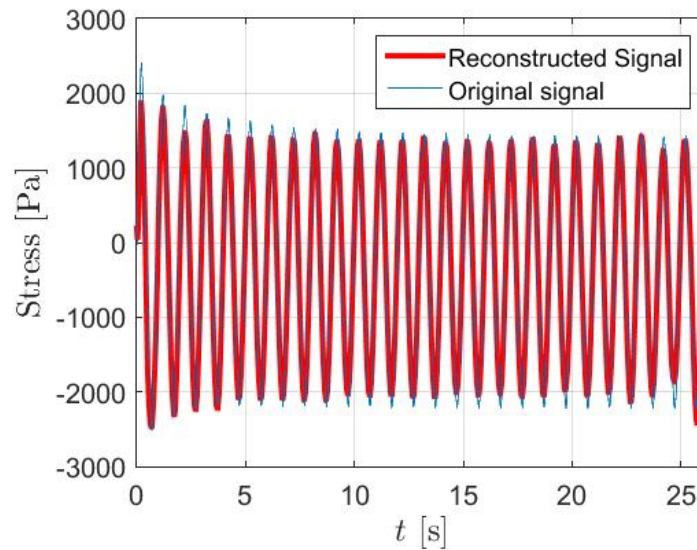


Figure 42: Harmonic wavelet decomposition curve (including only the binned wavelets from Table 5) and the original stress curve for aortic tissue under 0% compression and 1 Hz, 25% translational shear strain. (20515a)

An increase in bin number corresponds to a decrease in wavelet amplitude. An increase in  $k$  level corresponds with a further shift to a later time. The bin number captures the highest magnitude wavelet in bin number 1 with decreasing magnitudes as the bin number increases. In general at a fixed  $j$  level, the  $k$  values trend from

Table 6: Brain Tissue 40 Cycles at 33% Compression (12915a)

Bin number	$j$ level	$k$ level
1	4	0
3	4	1
7	4	2
11	4, 4, 4	4, 5, 14
12	4, 4, 4, 4, 4	3, 7, 8, 10, 11
13	4, 4, 4	6, 9, 13
14	4	12
16	4, 5, 6	15, 0, 1
17	6	0
18	6, 6	2, 3

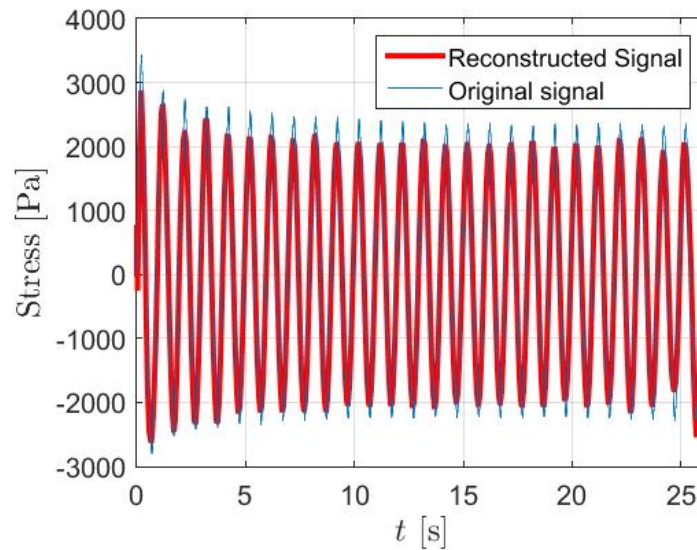


Figure 43: Harmonic wavelet decomposition curve (including only the binned wavelets from Table 6) and the original stress curve for aortic tissue under 33% compression and 1 Hz, 25% translational shear strain. (12915a)

low to high with respect to the bin number which correlates to the drop in amplitude with respect to time. The first 5 largest amplitudes are consistently  $j = 4$ , and low level  $k$ . Small  $k$  values correspond to the stress at the beginning of the response (first few cycles).

As described in Section 3.4.2, the bins are organized by magnitude. For all tests, Bin 20 contains a large amount of wavelets with the bottom 5% magnitudes. If a bin

Table 7: Aortic Tissue 40 Cycles at 0% Compression (22515b)

Bin number	$j$ level	$k$ level
1	4	2
2	4	1
3	4, 4	0, 14
4	4	5
5	4, 4, 4	4, 8, 11
6	4, 4, 4, 4, 4, 4	3, 6, 7, 9, 10, 13
7	4	12
8	4	15
17	5	0
18	-1	0
19	6	0

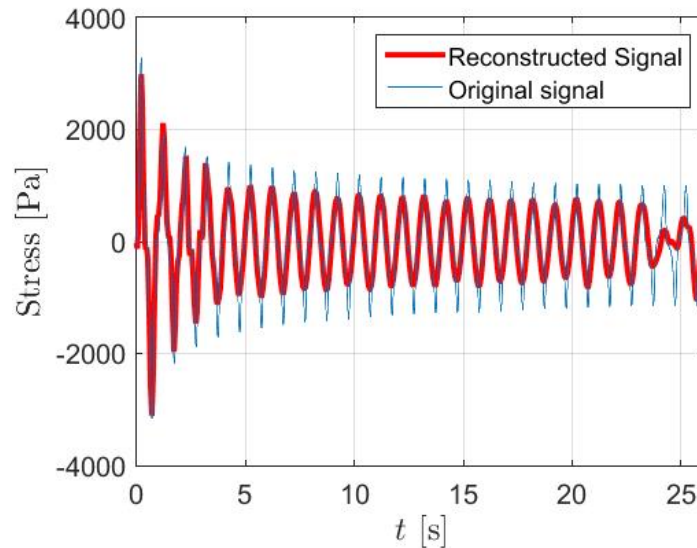


Figure 44: Harmonic wavelet decomposition curve (including only the binned wavelets from Table 7) and the original stress curve for brain tissue under 0% compression and 1 Hz, 25% translational shear strain. (22515b)

contains many wavelets (greater than 50), then the bin is not considered for analysis (This only happens for these tissue responses in the smallest magnitude bins, 19 and 20). Any other bin excluded from the tables above is due to the lack of any wavelets in that particular magnitude range.

The harmonic wavelet analysis successfully fits both tissue stress response curves as shown by the very low  $L_2$  Error for All Wavelets in Table 8 and Figure 41. The  $L_2$

Table 8: Aortic Tissue 40 Cycles at 33% Compression (22515d)

Bin number	$j$ level	$k$ level
1	4, 4	1,2
4	4, 4	0, 14
5	4, 4, 4	4, 5, 8
6	4, 4, 4	3, 7, 11
7	4, 4, 4, 4, 4	6, 9, 10, 12, 13
9	4	15
16	5	0
19	6, 7, 15	0, 0, 0

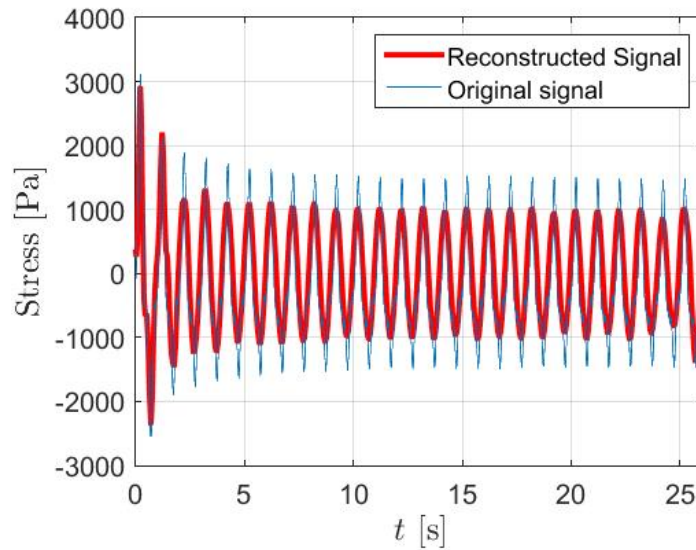


Figure 45: Harmonic wavelet decomposition curve (including only the binned wavelets from Table 8) and the original stress curve for brain tissue under 33% compression and 1 Hz, 25% translational shear strain. (22515d)

norm error (Equation 26) depicts the standard deviation as a relative fraction that contains a more obvious meaning. The  $L_2$  error for the binned wavelets (top 90% in magnitude) are low and show a good fit without using all wavelets (wavelets from Bin 20 are excluded). The harmonic wavelet decomposed artery stress response has a lower  $L_2$  error value than the brain stress response  $L_2$  error.



Table 9:  $L_2$  Error for Binned Wavelets and All Wavelets

Test	$L_2$ Error Binned Wavelets	$L_2$ Error All Wavelets
Artery, 0%		
22515b	0.1284	6.73E-08
22515c	0.1146	1.03E-08
40915a	0.0725	6.67E-09
40915b	0.0667	4.02E-08
40915c	0.0675	1.15E-08
40915d	0.0652	1.73E-09
AVG	0.0858	2.29E-08
SD	0.0280	2.55E-08
Artery, 33%		
22515d	0.1545	8.94E-09
22515e	0.106	1.42E-08
22515f	0.0913	1.53E-08
40915e	0.0707	5.51E-09
40915f	0.0701	8.73E-09
40915g	0.0933	1.62E-07
AVG	0.0976	3.58E-08
SD	0.0311	6.20E-08
Brain, 0%		
20515a	0.3517	8.73E-06
20515b	0.3567	2.89E-06
21915a	0.3723	3.28E-07
21915b	0.3563	4.37E-08
42315b	0.3605	2.16E-08
42315c	0.3626	5.62E-06
AVG	0.3600	2.93E-06
SD	0.007	3.58E-06
Brain, 33%		
12915a	0.4743	2.74E-06
42315d	0.3504	6.54E-09
42315e	0.318	1.06E-08
42315f	0.3343	3.29E-08
42315g	0.311	1.44E-08
42315h	0.237	7.02E-07
AVG	0.3375	5.83E-07
SD	0.0775	1.08E-06

#### 4.2.4 2 Hz Analysis

To verify that the shoulder response was not a phenomena of only a 1 Hz applied deformation, a test was completed at 2 Hz under 0% compression and 25% translational strain; the shoulders are still present (Figure 46). The Fourier series decomposition coefficients are given in Table 9.

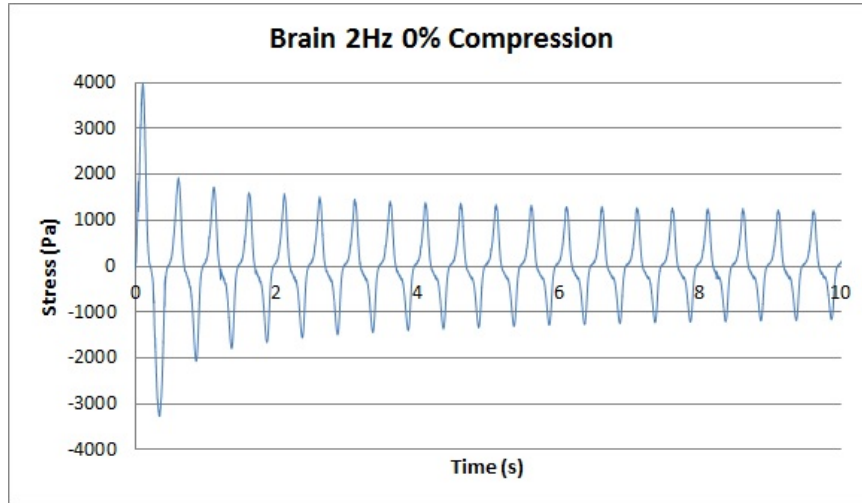


Figure 46: Stress versus time for brain tissue under 0% compression and 2 Hz, 25% translational shear strain.

Table 10: Fourier Coefficients for Brain Tissue 0% Compression and 2 Hz

Frequency	Fourier Coefficient Magnitude
0 Hz	30.8052
2 Hz	817.4784
4 Hz	43.5473
6 Hz	337.1983
10 Hz	96.2478

The dominant frequency values from the 2 Hz test are twice those obtained from the 1 Hz tests due to the doubling in applied deformation frequency. The 2, 6, and 10 Hz coefficients (Table 9, Figure 47) correlate to dominant 1, 3, 5 Hz components in the 1 Hz tests. Harmonic wavelet analysis has a fractional error of 0.2965 for the wavelets in bin 1-19. Table 11 shows the harmonic wavelet coefficients for the brain

tissue under an applied 2 Hz deformation frequency and 0% compression. A  $j$  level of 4 corresponds to 2 Hz and a  $j$  level of 6 corresponds to 6 Hz (Equation 25).

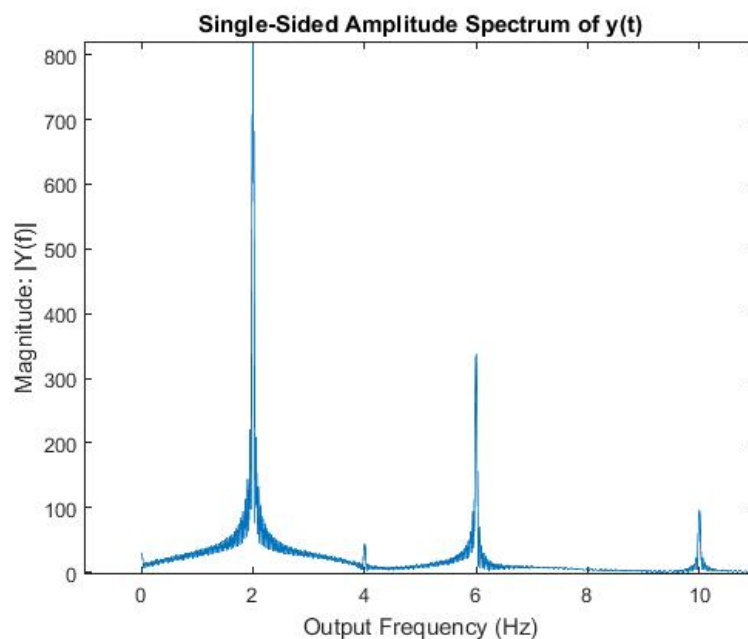


Figure 47: Fourier series decomposition coefficients versus frequency for brain tissue under 0% compression and 2 Hz, 25% translational shear strain.

Table 11: Harmonic Wavelet Coefficients for Brain Tissue at 0% Compression and 2 Hz

Bin number	$j$ level	$k$ level
1	4	0
4	4	1
11	4	2
14	4, 4, 5, 6	4, 5, 0, 1
15	4, 4, 4	3, 7, 8
16	4, 4, 4, 4, 4	6, 10, 11, 13, 14
17	4, 4	9, 12
18	5, 6, 6, 6, 6	1, 0, 2, 3, 4
19	4, 5, 6, 6, 6, 6, 6, 6, 6, 6, 6, 6, 6, 6, 6	0, 15, 5, 6, 7, 8, 9, 10, 11, 12, 14, 15, 16, 19, 24

#### 4.2.5 Results Summary

The stress response of bovine aortic tissue and rat brain tissue under combined unconfined compression and translational sinusoidal shear deformation exhibits many similarities. The first peak stress amplitudes (the largest peak in the signal) of both materials are statistically similar. The stress response for both materials displays a transient response and drop in stress magnitude after subsequent cycles. The brain tissue stress drops more in magnitude and more rapidly over the cycles than the aortic tissue stress response causing the brain tissue to have a lower steady state stress value. The aortic tissue stress response for some specimens slightly stiffens after 20 cycles; the brain tissue stress response does not display stiffening. Compression causes an increase in the stress response and an increase in the magnitude of the stress drop.

Neither stress response is in phase with the displacement and the brain tissue response exhibits a variable time shift (quasiperiodic). The brain tissue stress response leads the displacement response which differs from the lagging stress response of the aortic tissue. The aortic tissue stress response is nearly symmetric with respect to the vertical axis of one half cycle but the brain tissue stress response is not symmetric due to shoulders in the curve.

A Fourier series decomposition of the stress response of both materials detects a 1 Hz and 3 Hz component. Likewise, a harmonic wavelet decomposition captures how each frequency component changes with respect to time. The shoulders correspond to a 3 Hz component that exists throughout the signal of the brain tissue response; the aortic tissue stress response 3 Hz component does not persist throughout the signal. The Fourier 1 Hz component has a larger magnitude in the stress response of aortic tissue and the Fourier 3 Hz component has a larger magnitude in the stress response of brain tissue.

## 5 Discussion

The mechanisms underlying the mechanical response of either aortic or brain tissue are not yet definitively determined. Because both tissues are hydrated, the interstitial fluid probably plays a significant role in the mechanical response. The influence of the fluid-solid interaction appears in the transient stress response, the stress frequencies detected from frequency analyses and the shape of each stress versus time response, each of which is interpreted using the structural properties.

Aortic tissue can hold a translational shear stress due to the highly structured, layered form of the tissue (Section 2.2.1). The structure of brain tissue is much different than aortic tissue and is maintained by a balance between axonal tension and hydrostatic pressure (Van Essen, 1997). A possible explanation for how brain tissue holds a translational shear stress is that the hydrostatic pressure within the tissue increases with an applied unconfined compression or with an applied shear that causes distortion and that the axons tension increases to compensate for the pressure change. Since axons exist in all directions (Figure 48), an applied shear stress would cause some of those axons to stretch in tension. The increased tension in the axons could resist further stretch of the axons which may resist shear deformation.

A positive and negative mover direction is defined by the Wintest programming and refers to a relative center, or zero displacement (B), position (Figure 50, 52) of the Bose mover. The positive and negative displacement indicates the location of the mover, away (Figure 49 and point A in Figure 52) or toward (Figure 51 and point C in Figure 52), the Bose machine with respect to the center position. The center position is where the mover is located at the beginning of every test. A positive and negative stress is directly calculated from the detected load cell reading; a negative load indicates a compressive load from the bottom plate pushing on the load cell and a positive load indicates a tensile load. The displacement reading corresponds to the top surface of the specimen attached to the Bose mover and the load detected is the

specimen action on the bottom plate.

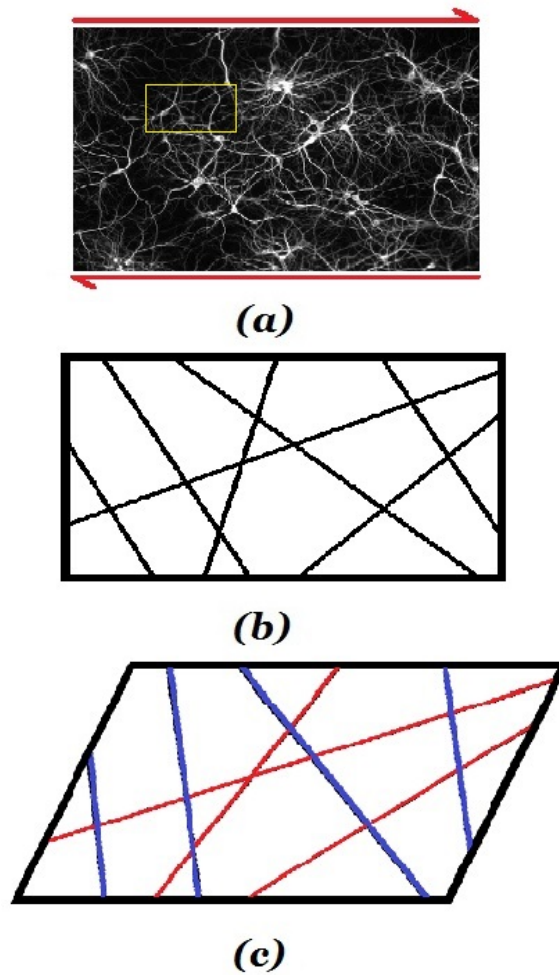


Figure 48: (a) Axons are oriented in all directions; each line in this schematic represents a possible direction of axons in undeformed brain tissue. (b) Schematic of a brain specimen in translational shear. Red lines represent directions that are in tension and blue lines represent compression (axons would be 'slack').

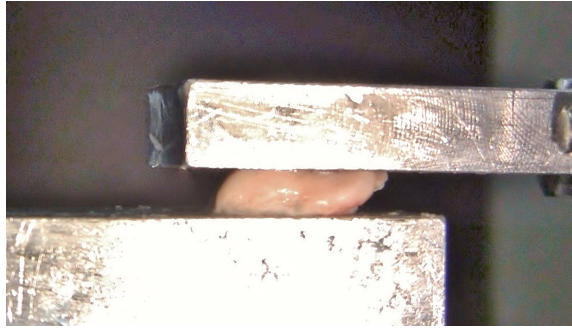


Figure 49: Brain tissue specimen at positive shear position corresponding to point A in Figure 52.

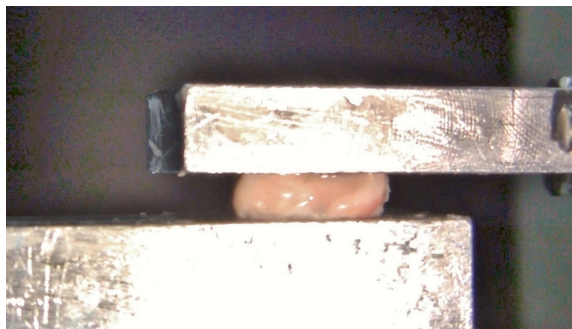


Figure 50: Brain tissue specimen at center shear position corresponding to point B in Figure 52.



Figure 51: Brain tissue specimen at negative shear position corresponding to point C in Figure 52.

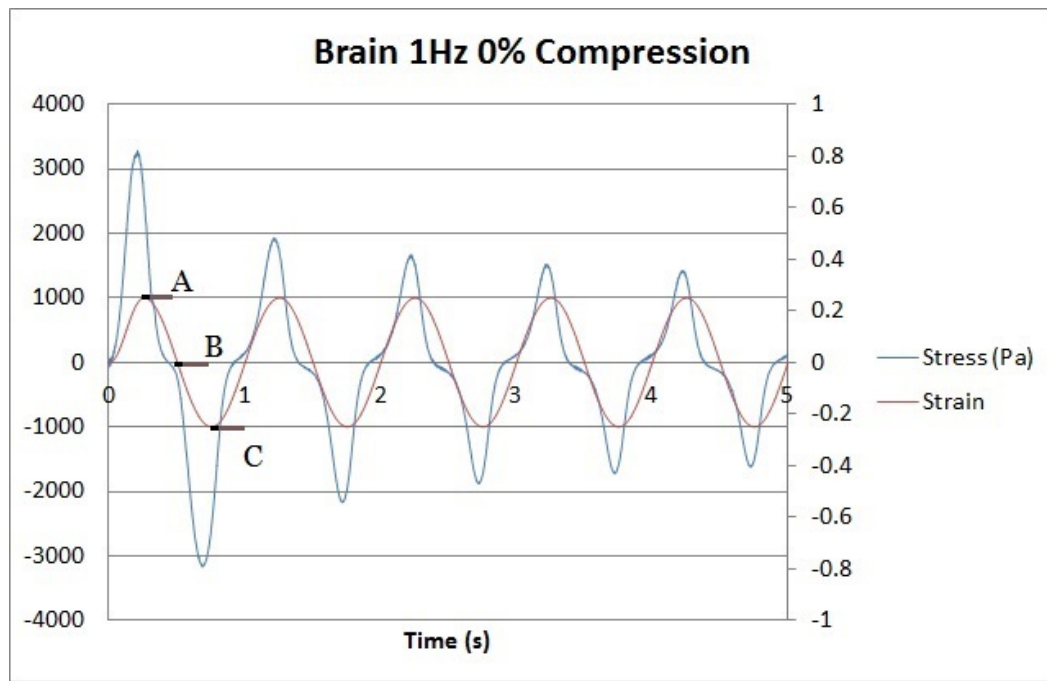


Figure 52: A is the positive shear position, B is the center, or zero, shear position, and C is the negative shear position. A, B, and C correspond to the position of the mover on each displacement cycle.



## 5.1 Solid-Fluid Interaction in the Mechanical Response

Brain tissue contains both solid and fluid phases that may affect the shear stress response of the tissue separately as well as interfere with each other. The extracellular space (ECS) of the brain contains and allows the extracellular fluid (ECF) to move. Normally, in vivo the ECF is known to transport nutrients and remove cell waste. Pulsing arteries cause a pressure differential that drive the fluid from the para-arterial to the paravenous pathways (Section 2.2.2). The volume and construction of the ECS controls the tortuosity, the measure of path curvature that the fluid must travel in a given physical length, of the tissue. To better explain the tissue's stress response, the behavior of the solid and fluid phases and their interaction will be interpreted during the applied deformation.

The solid-fluid interaction is defined by the influence that the fluid phase has on the solid phase of the material or vice versa. The solid phase can affect the fluid because an applied stretch of the solid phase may cause pressure differentials in the ECF and fluid redistribution. The fluid can affect the solid phase due to drag. A drag force is equal and opposite on the fluid and solid parts, but the fluid phase cannot hold a shear stress. Only the solid phase is connected to the load cell and therefore is the only phase that can create a stress from the load cell attached to the bottom grip. Drag can result from fluid friction on a surface of the solid matter wall or from fluid hitting the solid matter surface normal to the fluid flow.

Stress relaxation is largely due to fluid redistribution in hydrated viscoelastic materials such as brain tissue (Haslach et al. 2015a) or cartilage (Mow et al. 1980). A redistribution of fluid causes a decrease in pressure and therefore a drop in axonal tension and a drop in stress. Stress relaxation occurs after a deformation is applied and then fixed over time while the stress drops through time often to a steady state stress value. Since stress relaxation occurs at a fixed strain as fluid redistribution, fluid redistribution is likely to also occur in cyclic loadings. If the fluid within the

brain tissue structure redistributes from high pressure locations toward low pressure locations, the total stress supported would decrease over time. The stress relaxation may also be dependent on the moisture content in the aorta because hydration lowers the glass transition of elastin and causes the elastin to be rubbery at body temperature. Lillie and Gosline (1990) state that elastin, when dry, exhibits little elasticity and hydrated elastin exhibits significant elasticity.

## 5.2 Transient Response

Over the 40 cycles of applied deformation, the stress response of the brain and aortic tissue drops over the first few cycles and levels off to an apparent limit cycle. The transient stress response may be due to several different causes in aortic tissue than in brain tissue. The aortic tissue has residual stresses within the tissue *in vivo* that are lost once the specimen is cut. Rings that are slit gradually open over time probably because the residual stresses relax in the elastic sheets (Vaishnav and Vossoughi 1987, Rahal et al. 2006). The relaxation of residual stresses prior to testing may cause the transient response of aortic tissue possibly due to relaxed collagen fibers and elastin sheets prior to testing. *In vivo*, the aortic tissue would not exhibit a transient response because it is always undergoing cyclic loadings. If the aortic tissue has relaxed and is not in its natural, original *in vivo* stress carrying state, the stress response *in vitro* may be affected.

The brain tissue transient stress response may be due to a buildup of pressure within the tissue causing axonal stretch and possible axonal breakage which would change the tortuosity of the material. Damage of the solid matter could create additional pathways for the fluid to flow. The redistribution of the fluid could cause a decrease in pressure on subsequent loadings and therefore less axonal stretch which leads to a lower stress carrying ability. If the fluid carries hydrostatic pressures high enough to damage the solid state of the tissue, additional pathways would be cre-

ated rapidly which correlates with the stress peak drop that occurs quickly and in large magnitudes in the first few cycles. A theorized principle used throughout this discussion is the easier the fluid can flow, the lower the shear stress measured.

The transient stress response of both tissues is similar to the Mullins effect in rubber. The Mullins effect is speculated to be an effect due to bond breaking, and it is likely that aortic and brain tissue also experience bond breaking. The exponential fit equation (Equation 18) provides insight on how quickly the stress is dropping and by how much. The brain tissue drops quickly and in large magnitudes; this could be due to large quantities of axonal breakage and the opening of pathways in the tissue. The stress-strain curves help visualize the transient response as the loops change after each cycle (Section 4.1.6). The brain tissue stress-strain curves include just a few initial, transient curves that lie outside of an apparent ‘limit cycle’, but have a large difference in stress magnitude between those cycles whereas the aortic tissue does not have as large of a stress magnitude change on subsequent cycles after the transient response. This difference reflects the explanation given about the transient response and possible damage in the brain tissue during testing.

The limit cycle would be expected for the artery but not the brain; the aortic tissue is naturally cyclically loaded and brain tissue is not significantly loaded naturally. (The brain does experience small changes in pressure due to the pulsing arteries.) The limit cycle does not have a physiological explanation in the brain stress response. A steady state, or limit cycle in brain tissue, possibly occurs when the pressure buildup no longer causes axonal breakage and the ECF redistributes more freely.

### 5.3 Frequency Analysis

The harmonic wavelet decomposition analysis here is a novel application of the technique to the mechanical response of soft, hydrated, biological tissue and is successful in giving information about the material stress response. Harmonic wavelets have

previously been used in music analysis and signal analysis (Newland 1993, 1994a). Harmonic wavelets successfully fit the quasiperiodic, changing magnitude stress response, unlike Fourier series analysis. The harmonic wavelets have a significant non-zero magnitude during a finite time interval that differs from Fourier series analysis that uses infinite homogeneous magnitude sine waves. Harmonic wavelet decomposition analysis allows for the capture of change in magnitude and variable time shifts of each cycle.

Frequencies other than the expected 1 Hz and the harmonic 3 Hz components exist in the harmonic wavelet decomposition at the beginning of the signal ( $k = 0$ ) for aortic and brain tissue. These other frequencies could be due to the starting up of the Bose displacement mover or may be due to the breaking of bonds in the tissue. The 3 Hz component in both the Fourier series and harmonic wavelet decomposition corresponds to the appearance of a shoulder in the brain tissue stress response. The aortic tissue stress response does not exhibit a distinct shoulder like the brain tissue stress response, but does exhibit a smaller magnitude 3 Hz component. The shoulder does not occur on the first quarter cycle of initial loading, but otherwise the shoulder appears to maintain a similar shape throughout the cycles in the brain tissue tests. How the fluid may induce the shoulder in the brain tissue shear stress response is further examined below.

### **5.3.1 Fluid Influence on Brain Tissue Response during a Load-Unload Deformation Cycle**

The shear stress leads translational deformation in the brain tissue response. An increase in hydrostatic pressure and resistance to shear deformation could make the stress lead the displacement curves during the initial applied half sine wave. Axons have viscoelastic properties that when in tension exhibit a stress leading response, that is effectively modeled by Dennerll et al. (1989) using Zener's model, the Kelvin-

Voight model in series with a spring ( $R_1 = 4$  microdynes/ $\mu\text{m}$ ,  $R_2 = 9$  microdynes/ $\mu\text{m}$ ,  $\eta = 6,000$  microdynes\*s/ $\mu\text{m}$ ). The phase shift,  $\delta$ , is calculated from the parameters found by Dennerell et al. (1989) by solving the differential equations for the Zener model. The phase shift is converted to time by Equation 1. Using a fixed frequency of 1 Hz in Mathematica, the time shift calculated for an axon is 0.0000169s. This time shift due to axonal stretch is much smaller than the observed time shift in the brain tissue stress-time curve. The axonal material properties may cause some of the time shift within the data, but the remainder of the time shift is speculated to be due to the fluid. Time shift may be related to the viscoelastic response.

As the mover displacement starts to slow down to change directions at the peak of the first half sine (Figure 49, point A on Figure 52), the difference in hydrostatic pressure within the tissue due to a distortion of the extracellular space forces the fluid to redistribute and reduce hydrostatic pressure which causes a stress relaxation to occur because the zero velocity position is temporarily a fixed deformation. This fluid redistribution that is initiated by a slowing in the mover until the displacement approaches zero velocity could cause a drop in stress prior to the peak deformation which would cause stress to further lead prior to the peak of the deformation sine waves. If the fluid is driven to redistribute due to the pressure differential in the tissue, the axonal tension would decrease as the fluid moves to equalize the pressure difference and the stress would drop. As the mover stops (Figure 49, point A on Figure 52) and changes direction, the stress continues to relax due to further fluid redistribution while the solid state is at its most distorted configuration. As the mover begins to return toward its initial position (Figure 50, point B on Figure 52), axonal tension and tissue distortion decrease.

As the mover accelerates to the zero position (Figure 50, point B on Figure 52), the deformation rate reaches its fastest speed as the mover crosses through the zero position; this speed could be related to the slope of the stress response or to the

shoulder phenomenon (Figure 25). The shoulder includes the positions at which the displacement crosses through the horizontal axis (Figure 50, point B on Figure 52), i.e. where the mover is accelerating to its fastest speed. Due to a reduction of distortion in the extracellular space and fluid redistribution during the unloading initial half sine, the stress reaches zero before the mover reaches the zero position which creates a leading stress response. The stress therefore may have a new zero stress position, that may be related to permanent distortions in the tissue.

The mover speed and acceleration could cause an inertial force in the fluid or drag from the neurons as the fluid passes through the tortuous ECS of the material. The stress may lead the displacement due to the inertial effects caused by the mover's acceleration when the stress is zero. It may also be possible that, as the mover slows after passing the zero position, tissue inertia keeps the tissue force on the load cell from the bottom grip and contributes to an overshoot of negative stress after the half cycle is completed. When the deformation continues to the zero position, after the stress has already reached zero, the repositioned fluid and possibly permanently distorted tissue may now resist the shear deformation in the opposing direction causing the negative shear stress detected.

When the displacement is at the zero position (Figure 50, point B on Figure 52), the distortion of the ECS may not have fully recovered to its original condition (Figure 53). The distortion of the ECS may vary during the sinusoidal deformation and after repetitive loadings. A change in time shift after repeated loadings may indicate a change in tortuosity of the tissue creating an easier available pathway for the fluid to flow, which could be related to possible damage. The hydrostatic pressure may increase in the direction of initial loading and result in a higher stress in that direction possibly due to the fluid's initial redistribution and possible initial damage. The change in stress amplitude after repeated loadings may be caused by the breaking of some connections within the structure of the tissue.

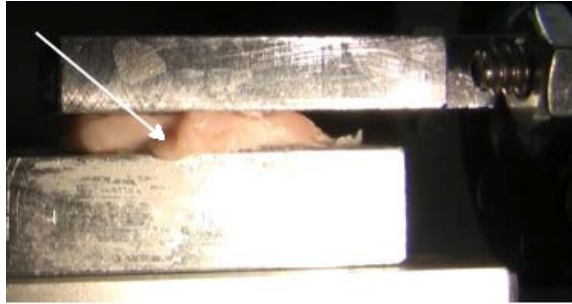


Figure 53: The arrow shows the rupture surface of brain tissue.

The shoulder is of great interest in the brain tissue stress response because it does not appear in aortic sinusoidal deformation and because it may indicate the role of the ECF in the mechanical response. The shoulder is closely related to the 3 Hz component detected from the harmonic wavelet decomposition analysis. The 3 Hz component may be due to a drag force of the fluid exerted on the solid phase. If the 3 Hz component is the stress component required to overcome drag, the bulk direction of fluid flow would be the same as the sign of the 3 Hz component at any given time because the force exerted from the ECF on the solid phase is in the direction of the ECF flow. The 3 Hz component magnitude decreases over the subsequent cycles in the harmonic wavelet decomposition, suggesting that the drag force may be smaller as the cycles continue which may be due to the fluid moving more easily. It is not definite that the drag force is responsible for all of the 3 Hz component because there are many other possible influences on the stress response of brain tissue such as stress relaxation, pressure differentials in the tissue, solid frictional forces between subsections, axonal damage and subsection shearing.

The shoulder does not occur on the initial loading in the first cycle. A possible explanation of the lack of a shoulder may be due to lack of damage during the initial cycle. Initially, the ECS has not been distorted by the load, but at each shoulder the ECS has been previously distorted. Only during the initial loading cycle does the displacement mover need to “start up” or accelerate up to speed since the mover cannot instantaneously move at the desired displacement rate. During the first loading,

the mover accelerates from the zero position because it is starting from rest, but on subsequent cycles the maximum velocity occurs at the zero displacement position and the mover decelerates during the loading. This start up may cause a slightly different displacement curve because of this acceleration period which may cause a different stress response.

### 5.3.2 Aortic Tissue Stress Response

Unlike the brain tissue stress response in which stress leads displacement, the aortic tissue stress response stress lags the displacement. When the aortic tissue specimen is cut, the residual stresses from the tissue holding a nearly circular shape are able to relax and the collagen fibers may crumple (no longer be stretched straight). At the beginning of the test, the mover displaces in the positive direction (Figure 49, point A on Figure 52) and for a small initial displacement the stress is very small which may indicate the small force and stretch required to elongate the collagen fibers from their crumpled state. Since the top surface of the tissue is controlled by the mover displacement and the bottom surface of the tissue is attached to the load cell to detect the load reading, the change in displacement direction of the top plate is not immediately reflected as a change in direction of the force on the load cell. The stress lag is due to the viscoelastic properties of the tissue which is comprised of elastin sheets, smooth muscle cells, and ECF. Recall, a purely elastic material would have stress and displacement in synchronization and a purely viscous material would have stress lagging by  $90^\circ$ ; Viscoelastic materials have a stress response that lags by a phase angle between  $0^\circ$  and  $90^\circ$ . The aortic tissue has a nearly constant time shift which differs from the brain tissue stress response which is quasiperiodic (non-constant time shift). The change in time shift is likely due to the damage in the brain tissue that does not occur in the aortic tissue.

As the displacement returns to the zero displacement position (Figure 50, point



B on Figure 52), the aortic tissue stress response does not have a distinct shoulder like the brain tissue stress response possibly because the material is more structured which may prevent the interstitial fluid from moving as easily. Aortic tissue in shear may prominently test the strength of the collagen, elastin and fibronectin that connects the smooth muscle cells and extracellular matrix (Section 2.2.1). This lack of an apparent shoulder in the aortic stress response correlates with the much smaller magnitude 3 Hz component from the Fourier series decomposition and harmonic wavelet decomposition analysis than the brain tissue stress response. If the 3 Hz component is the stress to overcome drag due to fluid movement, the small magnitude 3 Hz component from the aortic tissue stress response may correlate to the restriction of fluid causing less fluid motion throughout the tissue and a smaller drag force. Water is bonded to proteoglycans in aortic tissue near the smooth muscle cells which may prevent some fluid from moving. In aortic tissue, the fluid does not have a significant role in the structure of the tissue, unlike brain in which the structure is due to the balance of hydrostatic pressure and axonal tension.

An additional possible explanation for the shape of the aortic tissue response is tissue stiffening (Section 2.2.1). In the stress strain loops, the initial less steep slope at smaller strains correlates to the higher frequency components in the stress versus time graphs. This change in slope as the strain increases may be due to material properties of the aortic tissue; Clark and Glagov (1985) state that the aortic stress response hardens because of the matrix mat. Both the restricted fluid flow and the material stiffening could contribute to the small 3 Hz component.

The aortic peak stress response decreases with time in the in vitro tests but is not expected to occur in vivo, however a transient response may occur because prior to testing the residual stresses have relaxed which puts the specimen in a slightly different state. Fluid loss has been seen in aortic tissue ring inflation tests (Haslach 2011, 2015b). Some aortic tissue tests exhibit slight stiffening after many cycles which

may be due to the fluid being driven out of the specimen causing tissue dehydration; this is not likely to occur in vivo where the body is able to rehydrate the tissue.

## 5.4 Role of Compression

Fixed compression normal to the shear deformation increases the magnitude of the shear stress response of both tissues. In the brain, this may be due to an increase in ECF pressure when compressed. In the aortic tissue, compression may cause initial elongation of collagen fibers and smooth muscle cells which would create a higher stress under the same applied shear because the fibers may have a higher stretch magnitude. The stress drops more quickly and in larger magnitudes in the brain tissue stress response when compressed possibly due to a larger amount of damage due to the higher internal pressures. The aortic tissue stress response drops more quickly and in larger magnitudes when compressed possibly due to the fluid driven out of the specimen more rapidly due to internal pressures. The amount of stress drop and the quickness of drop is larger in the brain tissue stress response than in the aortic tissue stress response probably due to the damage that occurs in brain tissue and fluid redistribution which would occur rapidly whereas the aortic tissue response is very structured and may not be damaging.

The steady state stress value under compression for aortic tissue is larger than that of the steady state stress value for brain tissue perhaps because the aortic tissue holds its structural integrity whereas the brain is likely damaged under similar applied conditions. Brain tissue in vivo is not expected to hold a stress through time and meet an apparent limit cycle, however there may be a balance between the amount of damage and the fluid flow creating a drag force after several cycles. The brain tissue steady state stress is larger under compression which may be due to an increase in frictional force between subsections that may slide over one another or a tightening of pathways for the fluid to flow. Under compression, a higher force is required to

maintain the 1 Hz deformation with an amplitude of 25% strain.

## 5.5 Clinical Applications

Fibrous astrocytes connect white matter in the brain to the capillary walls at the blood brain barrier. The differing responses of cranial artery and brain tissue response under the same applied conditions could cause an immediate shearing between the tissues during an external insult and may cause disruptions between the interfaces of these tissues including the blood-brain barrier (Section 2.2). Because of a difference in matter density, interfaces between grey and white matter usually damage easier causing “hemorrhages [to be] characteristically located at the gray-white matter interface” (Wasserman 2014). The density and mechanical response differences may cause damage between arterial and brain connections. The loss in load carrying ability of brain tissue may be due to the breaking of neuron-neuron or neuron-gial connections due to excessive ECF pressure, leading to symptoms of mild traumatic brain injury (mTBI), especially in the hippocampus. After some of these connections are broken, the fluid is able to move easier resulting in a lower overall ECF pressure.

The results suggest that the fluid content has a large influence on the stress response of the tissue and should lead to future testing to further examine how the fluid moves during mechanical deformation of the brain tissue. Tests that could track fluid movement would provide further information on the solid-fluid interaction during an applied force. Future work should be directed at a mathematical explanation of the 3 Hz response in terms of the drag force in the brain tissue.

## 5.6 Shortcomings or Limitations

A few limitations are noted for the test protocol. The unconfined compression was applied before the shear was applied due to the fixture design limitations. The Vet-bond had to be placed in a thin enough layer that it did not ride up the sides of the

specimen, but a thick enough layer for the specimen not to shear off of the plates. The tuning for the feedback loop of the Wintest 4.1 program for each tissue is not exact because Wintest approximates tuning based on linear elastic properties. Specimen variability exists for the thickness of aortic tissue because the natural thickness changes around a ring.

## 6 Conclusion

During trauma resulting from impacts and blast waves, sinusoidal waves permeate the brain and cranial arterial tissue, both non-homogeneous biological tissues with high fluid contents. Aortic tissue, used to model cranial arteries, is much more structured by the bonds between substructures, but the brain tissue structure is maintained by a balance of pressure and axonal tension. Both tissues exhibit Mullins effect in shear and have an apparent limit cycle. Harmonic wavelet decomposition shows significant 1 Hz and 3 Hz components. The 3 Hz component magnitude in brain tissue, which is much larger than in aortic tissue, may correlate to interstitial fluid induced drag forces that decrease on subsequent cycles perhaps because of damage resulting in easier fluid movement. Compression increases the stress response of both tissue and the hydrostatic pressure in brain tissue. A shear deformation causes the pressure inside the tissue to grow possibly because the fluid is unable to redistribute at a comparable rate. This pressure buildup is probably highly deformation rate dependent and may cause disruptions in the connections between substructures of the brain tissue. The difference between and mismatch of the responses of the arterial and brain tissues may cause damage between the connections of these two cranial tissues during external insults.

## 7 Appendix

### 7.1 Matlab Code

#### 7.1.1 Mullins Effect

The initial step for the Mullins effect analysis is a matlab code written to determine the positive peak stress peak values for each test and the time corresponding to each peak stress. Starting guesses for the  $A$ ,  $b$ , and  $c$  values are needed to use “lsqcurvefit” to fit the equation  $y = A \exp bt + c$  to the peak values. Different results are possible if different initial guess points are taken so it is essential to choose the guess point to fit the curve correctly.

#### 7.1.2 Time Shift

The time shift is determined from a matlab code that defines a ratio for all points as  $\text{stress}(i+1)/\text{stress}(i)$ , for  $i = 1, \dots, n$  for  $n$  number of total points, where stress is

$$\sigma = 10^{-3} \frac{g\mathcal{F}}{\mathcal{A}} \quad (28)$$

where  $\mathcal{F}$  is the detected load in grams,  $\mathcal{A}$  is the cross-sectional area of the specimen parallel to the test plate (in  $m^2$ ), and  $g$  is the gravitational constant. When this ratio is negative, this indicates where the stress curve crosses the horizontal axis. Linear interpolation approximation determines the time that each curve crosses the horizontal axis. The matlab output is the difference between the time that the stress crosses the horizontal axis and the time that the strain crosses zero (time is known and fixed from the programmed frequency), defined as  $\Delta t$ .

### 7.1.3 Filter Analysis

The pass filter analysis matlab code uses the command `idealfilter(f,t,interval, 'pass')` which is analyzed at a defined interval on the data. The stress and time data as well as the interval for the pass filter defined in Hz are input into the program, and the code outputs a graph of original data and the filtered data. The ideal filter command uses a range for the filter interval, which was set from 1-3 Hz.

### 7.1.4 Fourier Series

The Fourier series decomposition matlab code was written to determine the Fourier series frequencies, coefficients, and phase shifts. The input values for the code are the time and stress data, and the number of points per second. The code outputs several graphs including the magnitude frequency spectrum, the real and imaginary frequency spectrum, the reconstructed Fourier series and the original signal. This code uses the fast Fourier transform command to analyze the discrete data.

### 7.1.5 Harmonic Wavelet Analysis

The Harmonic wavelet analysis code has an input of time and stress from the original data, and outputs of the original signal graph, the reconstructed 20 bins organized by magnitude of wavelets, the final reconstructed signal aligned with the original signal, the total time analyzed, the  $L_2$  norm for the reconstructed fit, the maximum and minimum load values of sine signal, and the 20 bin wavelet coefficients for each  $j$  and  $k$  level. This code uses the fast Fourier transform command as well as the inverse fast Fourier transform to perform the harmonic wavelet analysis, as outlined in Newland (1994b).

### 7.1.6 Wavelet Examination

An additional matlab code was created to better examine a particular wavelet with given  $a$ -values (where  $a$  is the complex magnitude of the wavelet). The code inputs the values determined from the harmonic wavelet analysis into equation

$$Y = 2 \operatorname{real}(a) \frac{\sin(4\pi x) - \sin(2\pi x)}{2\pi x} - 2 \operatorname{imag}(a) \frac{[\cos(4\pi x) - \cos(2\pi x)]}{2\pi x} \quad (29)$$

to graph the single wavelet with respect to time.



## 7.2 Planes of Dissection

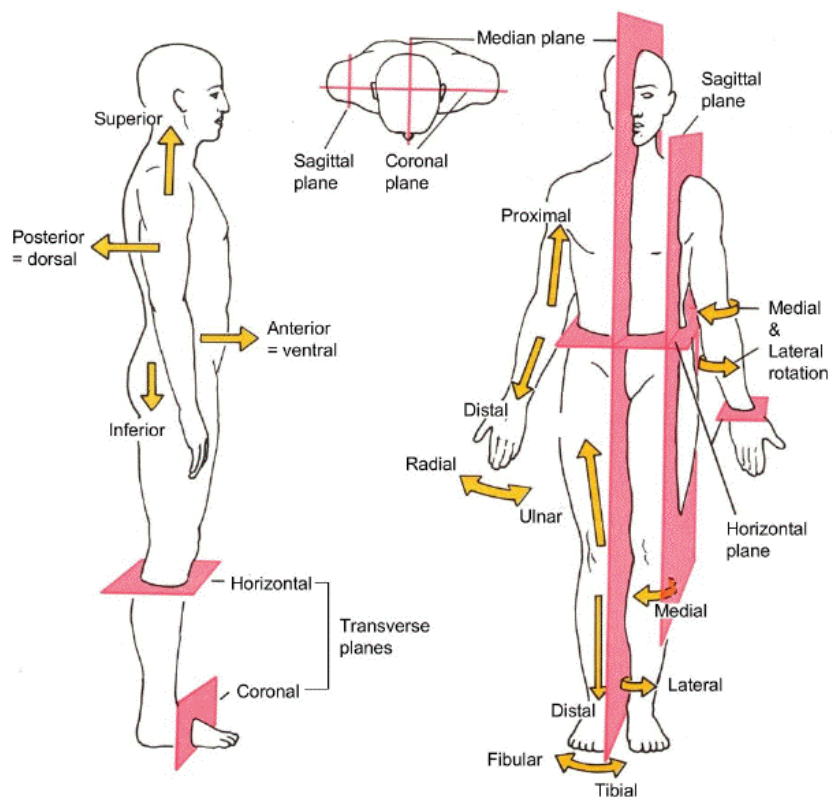


Figure 54: Planes of Dissection (Zimmerman 2015)

## 8 References

- [1] S. Baek, R. Gleason, K. Rajagopal, and J. Humphrey (2007). Theory of small on large: Potential utility in computations of fluid-solid interactions in arteries. *Computer methods in applied mechanics and engineering* **196**, 3070-3078.
- [2] A. Bain, and D. Meaney (2000). Tissue-level thresholds for axonal damage in an experimental model of central nervous system white matter injury. *Journal of Biomechanical Engineering: ASME* **122**, 615-622.
- [3] A. Blanchard, and D. Parkinson (1952). Breakage of carbon-rubber networks by applied stress. *Journal of Industrial and Engineering Chemistry* **44**, 799-812.
- [4] F. Bueche (1960). Molecular Basis for the Mullins Effect. *Journal of Applied Polymer Science* **4**, 107-114.
- [5] J. Campellone (2015). Circle of Willis: MedlinePlus Medical Encyclopedia Image. *U.S. National Library of Medicine*, Web. 16 July 2015.
- [6] R. Chan, and M. Rodriguez (2008). A simple-shear rhometer for linear viscoelastic characterization of vocal fold tissues at phanatory frequencies. *The Journal of the Acoustical Society of America* **124**, 1207-1219.
- [7] J. Clark, and S. Glagov (1985). Transmural Organization of the Arterial Media: The Lamellar Unit Revisited. *Journal of the American Heart Association: Arteriosclerosis, Thrombosis, and Vascular Biology* **5**, 19-34.
- [8] E. Davis (1993). Smooth muscle cell to elastic lamina connections in developing mouse aorta. *Lab Invest.* **68**, 89-99.
- [9] T. Dennerll, P. Lamoureux, R. Buxaum, and S. Heidemann (1989). *The Journal of Cell Biology* **109**, 3073-3083.
- [10] J. Diani, M. Brieu, and J. Vacherand (2006). A damage directional constitutive model for Mullins effect with permanent set and induced anisotropy. *Eur Journal of Mechanics and Physics of Solids* **25**, 483-496.
- [11] K. Dingemans, P. Teeling, J. Lagendijk, and A. Becker (2000). Extracellular

- matrix of the human aortic media: An ultrastructural histochemical and immunohistochemical study of the adult aortic media. *The Anatomical Record* **258**, 1-14.
- [12] R. Greenspan (2015). CBAM fosters innovative research into novel technologies aimed at obtaining a full picture of the brain's signaling activities. *UC San Diego: Center for Brain Activity Mapping*, Web. 12 August 2015.
- [13] D. Haskett, G. Johnson, A. Zhou, U. Utzinger, and J. Vande Geest (2010). Microstructural and biomechanical alterations of the human aorta as a function of age and location. *Biomech Model Mechanobiol* **9**, 725-736.
- [14] H. Haslach, P. Riley, and A. Molotsky (2011). The Influence of Medial Substructures on Rupture in Bovine Aortas. *Journal of Cardiovascular Engineering and Technology* **2** 372-387.
- [15] H. Haslach, L. Leahy, and A. Hsieh (2015a). Transient solid-fluid interactions in rat brain tissue under combined translational shear and fixed compression. *Journal of the Mechanical Behavior of Biomedical Materials* **48**, 12-27.
- [16] H. Haslach, L. Leahy, P. Fathi, J. Barrett, A. Heyes, T. Dumsha, and E. McMahon (2015b). Crack Propagation and Its Shear Mechanisms in the Bovine Descending Aorta. *Cardiovascular Engineering and Technology* 1-18.
- [17] G. Holzapfel, T. Gasser, and R. Ogden (2000). A new constitutive framework for arterial wall mechanics and a comparative study of material models. *Journal of Elasticity* **61**, 1-48.
- [18] L. Horný, E. Gultová, H. Chulp, R. Sedláček, J. Kronek, J. Veselý, and R. Žitný (2010). Mullins Effect in Aorta and Limiting Extensibility Evolution. *Bulletin of Applied Mechanics* **6**, 1-5.
- [19] J. Humphrey, and S. Na (2002). Elastodynamics and Arterial Wall Stress. *Annals of Biomedical Engineering* **30**, 509-523.
- [20] J. Iliff, M. Wang, Y. Liao, B. Plogg, W. Peng, G. Gundersen, H. Benveniste,

- G. Vates, R. Deane, S. Goldman, E. Nagelhus and M. Nedergaard (2012). A paravascular pathway facilitates CSF flow through the brain parenchyma and the clearance of interstitial solutes, including Amyloid  $\beta$ . *Science Translational Medicine* **4**, 1-10.
- [21] M. Lillie, and J. Gosline (1990). The effects of hydrations on the dynamic mechanical properties of elastin. *Biopolymers* **29**, 1147-1160.
- [22] W. Mars, and A. Fatemi (2004). Observations of the constitutive response and characterization of filled natural rubber under monotonic and cyclic multiaxial stress states. *Journal of Engineering Mathematics and Technology* **126**, 19-28.
- [23] T. Mathiisen, K. Lehre, N. Danbolt, and O. Ottersen (2010). The perivascular astroglial sheath provides a complete covering of the brain microvessels: An electron microscopic 3D reconstruction. *Glia* **58**, 1094-1103.
- [24] V. Mow, S. Kuei, W. Lai, and C. Armstrong (1980). Biphasic Creep and Stress Relaxation of Articular Cartilage in Compression: Theory and Experiments. ASME. *Journal of Biomechanical Engineering* **102**, 73-84.
- [25] D. Newland (1993). Harmonic Wavelet Analysis. *Proceedings: Mathematical and Physical Sciences* **443**, 203-225.
- [26] D. Newland (1994a). Harmonic and Musical Wavelets. *Proceedings: Mathematical and Physical Sciences* **444**, 605-620.
- [27] D. Newland (1994b). Wavelet Analysis of Vibration, Part I: Theory and Part II: Wavelet Maps. *Journal of Vibration and Acoustics* **116**, 409-425.
- [28] E. Pena (2011). Predication of the softening and damage effects with permanent set in fibrous biological materials. *Journal of the Mechanics and Physics of Solids* **59**, 1808-1822.
- [29] E. Pena, and M. Doblare (2009). A anisotropic pseudo-elastic approach for modeling Mullins effect in fibrous biological materials. *Mechanics Research Communications* **36**, 784-790.

- [30] A. Rachev, and K. Hayashi (1999). Theoretical Study of the Effects of Vascular Smooth Muscle Contraction on Strain and Stress Distributions in Arteries. *Annals of Biomedical Engineering* **27**, 459-468.
- [31] D. Rehal, X. Guo, X. Lu, and G. Kassab (2006). Duration of No-Load State Affects Opening Angle of Porcine Coronary Arteries. *American Journal of Physiology: Heart and Circulatory Physiology* **290**, H1871-H1878.
- [32] Seward (2015). North Carolina State University: Lab 3 Cranium. Web. 16 July 2015.
- [33] D. Silverthron (2013). Ch. 9: The Central Nervous System. *Human Physiology: An Integrated Approach*. Prentice Hall.
- [34] The Jackson Laboratory (2015). MGI- Mouse Genome Informatics - The International Database Resource for the Laboratory Mouse: The Anatomy of the Laboratory Mouse. Web. 16 July 2015.
- [35] University of Utah: Health Sciences (2015). Animal Models for Addiction Research. Web. 16 July 2015.
- [36] R. Vaishnav, and J. Vossoughi (1987). Residual Stress and Strain in Aortic Segments. *Journal of Biomechanics* **20**, 235-239.
- [37] D. Van Essen (1997). A tension-based theory of morphogenesis and compact wiring in the central nervous system. *Nature* **385**, 313-318.
- [38] A. Verkman (2013). Diffusion in the extracellular space in brain and tumors. *Physical Biology* **10**, 1-8.
- [39] J. Wasserman (2014). Diffuse Axonal Injury Imaging : Overview, Radiography, Computed Tomography. Web. 16 July 2015.
- [40] I. Zimmerman (2015). Body Planes *Isaiah's Anatomy Website*. Web. 16 July 2015.
- [41] A. Zuniga, and M. Beatty (2002). A new phenomenological model for stress-softening in elastomers. *Zeitschrift fur angewandte Mathematik und Physik*

